MSK1 expression in the GABAergic network and its relationship with striatal growth, BDNF-mediated MeCP2 phosphorylation and schizophrenia

Natalia Varela-Andrés[1,2,3,#], Alejandro Cebrián-León[1,2,3,#], Carlos Hernández del Caño[1,2,3,#], Inés S. Fernández del Campo[1,2,3], Sandra García-Losada[1,2,3], Noelia Martín-Ávila[1,2,3], Juan Carlos Arévalo[1,2,3], Miguel Merchán[1,2,3], Manuel Sánchez-Martín[3,4], Rubén Deogracias[1,2,3].

Authors affiliations:

1. Institute of Neurosciences of Castilla y Leon (INCyL), University of Salamanca, Salamanca, Spain.

2. Department of Cell Biology and Pathology, Faculty of Medicine, University of Salamanca, Salamanca, Spain.

3. Institute of Biomedical Research of Salamanca (IBSAL), Salamanca, Spain.

4. University of Salamanca, Salamanca, Spain.

# These authors contributed equally to this work.

* Corresponding author: Ruben Deogracias. Institute of Neurosciences of Castilla y Leon, C/Pintor Fernando Gallego 1, 37007, University of Salamanca, Salamanca, Spain. rdeogracias@usal.es

Keywords: BDNF, MSK1, MeCP2, striatum, neuronal development, schizophrenia.

Significance statement

Brain development requires, at a cellular level, the coordinate action of extrinsic and intrinsic regulating factors to control the correct assembly of neuronal networks. Although much attention has been focussed on the action of extrinsic factors such as BDNF, it is still unclear how this neurotrophin is able to modulate responses in different cells. Here, through the analysis of a new *Msk1 KO* mouse model we identify a key role for MSK1, a kinase of the BDNF/MAPK pathway. We found that its expression is regulated during mouse brain development in GABAergic neurons. Through this approach, we have shown that MSK1 is an essential intrinsic factor of GABAergic neurons, participating during development in the control of striatal Medium Spiny Neurons arborization, in the activity of MeCP2, and in the expression of genes involved in the GABA and dopamine regulation in the striatum. Our

results also demonstrate that the actions of MSK1 are essential for proper maturation of the striatal circuits and its absence can be related with schizophrenia-like symptoms in adult mice.

Abstract

It is becoming evident that impairments of the neuronal circuitry during development are the basis for some human disorders including autism and schizophrenia. To understand how synaptic wiring is formed and maintained is not only a major scientific challenge, but also has an important biomedical implication. The striatal GABAergic projection neurons, also called Medium Spiny Neurons (MSNs), represent more than 95% of the neuronal population in the striatum. This inhibitory brain hub is associated to voluntary body movements, reward-associated learning, and social behaviour control. The functional loss of the striatum has been associated with several neurological disorders including Huntington disease, Rett syndrome, and schizophrenia. The aetiology of these pathologies implies not only a decrease in the glutamatergic and dopaminergic inputs that reaches into the striatum, but also alterations of the GABAergic brain circuits occurring during development. Using a new MSK1 knockout murine model, we describe that mitogen- and stress-activated protein kinase-1 (MSK1) controls MSNs arborization during mouse brain development, phosphorylation of serine 421 in methyl-CpG binding protein-2 (MeCP2) and regulation of genes involved in gamma-aminobutyric acid (GABA) and dopamine functions, factors that finally cause behaviours reminiscent of schizophrenia in patients.

Introduction

During brain development, both extrinsic and intrinsic factors play a crucial role in shaping neural circuits and establishing connectivity patterns between neurons. Neurotrophins, in particular the brain-derived neurotrophic factor (BDNF) (1–5), neurotransmitters such as GABA, glutamate or dopamine (6–10), DNA-binding proteins such as

MeCP2 (11–13) or transcription factors like cAMP/$Ca2^+$ response element-binding protein (CREB) (14–16) stand out. These molecules work together to ensure the proper formation and organization of neural circuits and control precise synapse formation. Impairments in the signalling of these factors, are the basis for some of the most devastating human neurodevelopmental disorders, such as autism spectrum disorder, Rett Syndrome and schizophrenia (SCZ) (17, 18).

The striatum, whose neuronal content consists of 98% GABAergic projection neurons so-called MSNs, is the most important inhibitory hub of the brain. It plays a crucial role in reward processing and cognitive function, as well as in the selection of actions, the acquisition of motor skills, and emotions. Alterations in the migration, maturation and/or connectivity of striatal neurons have been found to contribute to the cognitive symptoms of SCZ (19). This cognitive dysfunction involves disruption of dopamine receptors expression in the striatum (19, 20), as well as the reduction in GABAergic transmission due to alterations in the GABA synthesis pathway (3, 21). These alterations result in a decrease of GABAergic synapses formed by interneurons, a relevant feature shown in patients with schizophrenia (10, 21–24). Several studies are beginning to shed light on the molecular mechanisms involved in the pathophysiology of schizophrenia, which are related with proper wiring of cortical and striatal GABAergic neurons (25–28).

The use of conditional mouse models lacking BDNF in the central nervous system (CNS) has shown that GABAergic neurons have an intrinsic program, absent in some classes of glutamatergic neurons, through which BDNF controls striatal growth and MSNs arborization (29–31). Among the signalling pathways that mediate these effects, the MAPK pathway is particularly interesting as it is implicated in MSNs arborization (29, 32–34), together to the proteins Ribosomal S6 Kinase family (RSK1, RSK2, RSK3) and the Mitogen- and Stress- activated Protein Kinase family (MSK1, MSK2) (35–39). MSK1 is recruited to

immediate-early gene (IEG) regulatory regions (40), where it phosphorylates Histone H3 and CREB (41), to expand the dynamic range of synapses in the hippocampus (42). Studies with adult mice lacking MSK1 and MSK1/MSK2 have shown that MSK1 is involved in the experience-dependent enhancement of mental ability, neuronal function and cognitive performance (41, 43). Additionally, cocaine administration has been shown to activate MSK1 in the striatum *in vivo,* while *Msk1 KO* mice exhibit an increased response to low doses of this drug, indicating the potential role of MSK1 in modulating neuronal responses (44, 45).

The production of GABA depends on the activity of the enzymes GAD65 and GAD67, which are required for the proper maturation and functionality of inhibitory circuits in the cerebral cortex (27, 46). Despite BDNF regulates CREB activity both in glutamatergic and GABAergic neurons, the expression of GAD65 and GAD67 is controlled by a specific gene program dependent on BDNF and CREB activation (3). Also, it has been reported an impairment in the expression of GAD65 and GAD67 in mice lacking MeCP2 only in GABAergic neurons, (47, 48). GABAergic neurotransmission is also affected in schizophrenia, what has been related to low levels of the GABA synthesising enzymes (27, 46). Therefore, it seems clear a correlation between BDNF/MAPK-dependent maturation of GABAergic neurons and some neurodevelopmental disorders. However, the intrinsic molecular program by which GABAergic neurons extend their axons and regulate some of their functions through the BDNF/MAPK pathway remains unclear.

MSK1 regulates BDNF-dependent CREB phosphorylation and gene transcription. Therefore, we hypothesized that MSK1 could play an important role during mouse brain development. For it, we analysed in mice the expression pattern of MSK1 at early postnatal ages and found to be high in both GABAergic cortical interneurons and MSNs. Surprisingly, MSK1 expression on these types of neurons is

differentially regulated until adulthood. To continue the study of the role of MSK1, we generated a new *Msk1* KO mouse line (*Msk1*^{IV} KO), what resulted in a significant impact on the growth of the striatum and BDNF-dependent arborization of MSNs along postnatal development. Furthermore, we found that MSK1 interacts with MeCP2 to control its BDNF-dependent phosphorylation and the regulation of genes involved in GABA and dopamine responses in the striatum. Finally, we observed that the lack of MSK1 alters the innate and specific social responses, anxiety and depressive behaviours in males and females mice without affecting their locomotor activity. These behavioural features are strongly reminiscent of phenotypes observed in schizophrenia patients.

Results

Msk1 expression changes during early postnatal mouse brain development.

To study the expression pattern of *Msk1* during mouse brain development, we analysed both the striatum and the somatosensory cortex between postnatal days P5 to P30 by qPCR and western blot assays (Fig. 1A and B). *Msk1* transcript levels are drastically reduced in the somatosensory cortex between P5 to P10, reaching nearly half of the amount of its levels at P30 (Fig. 1A). However, we observed a significant increment of *Msk1* mRNA levels in the striatum during all the analysed time points, with two significant increments between P5 to P10, and between P15 to P30 (Fig. 1A). MSK1 protein levels vary following a similar expression pattern to its transcripts at the same time points in both brain areas (Fig. 1B). MSK1 is therefore required during postnatal mouse brain development of GABAergic neurons, although its expression remains high just in MSNs in the adult brain. These data suggest a different role of MSK1 in both type of neurons.

MSK1 is mostly restricted to GABAergic neurons.

The changes observed on MSK1 protein levels during brain development might not be uniform throughout all the cells in the

somatosensory cortex and the striatum. In the adult mouse brain MSK1 is expressed by dopamine- and cAMP- regulated phosphoprotein, 32 kDa (DARPP-32) positive MSNs (49) and by few neurons in the cortex (50). We hypothesized that MSK1 expression could be mostly restricte to GABAergic interneurons, while in the striatum MSK1 could be expressed by the GABAergic MSNs. To assess this, we used the *Vgat-IRES-CRE; Ai9-RCL^{tdTomato} (Vgat-CRE; Ai9)* double mutant mice and quantified, by immunostaining, the degree of colocalization between tdTomato^{+} GABAergic neurons and MSK1^{+} cells in the cortex and striatum at postnatal ages P5, P10, P15 and P30 (Fig. 1C to 1H and Fig. S1 and S2). The low percentage of tdTomato interneurons that express MSK1^{+} at P5 in the somatosensory cortex (≈32%) decreases sharply at P10 (≈21%), and until P30 (≈3%) (Fig. 1C and D and Fig. S1). Around 85% of the GABAergic neurons in the somatosensory cortex express MSK1 at P5, a number that decreases to less than 40% at P30 (Fig. 1E). However, there are ≈60% on the number of striatal cells expressing MSK1 at P5 and P10, and a reduction to ≈40% at P30 (Fig. 1G and Fig. S2). Of these cells, approximately 96% are GABAergic neurons from P5 to P30 (Fig. 1H). Altogether, these results reveal that MSK1 expression is mostly restricted to GABAergic neurons in the somatosensory cortex and the striatum. Moreover, our data show that *Msk1* expression is differentially regulated during postnatal brain development in both brain areas.

Morphometric and densitometric analysis of striatal MSK1^{+} cells along postnatal development.

To analyze changes in MSK1 immunoreactivity in various stages of the mouse brain development, we used MATLAB maps coding area (Fig. 2 and Fig. S3) to determine the optical density (OD) values of MSK1^{+} cells correlated with its topographical distribution along the striatum, as previously reported (51). Between P5 to P10 the number of MSK1^{+} cells per 1000μm^2 significantly decreases, although at P10 cells show

much higher OD. At P15, the number of immunoreactive cells increases again to values higher than P5 and P10, while OD decreases to the same level as in P5. Finally, at P30 we found the highest amount of $MSK1^+$ cells per 1000μm^2 (Fig. S3). OD values at this stage are lower than at P10, but higher than at P5 and P15 (Fig. S3). The mean area of the immunoreactivity in $MSK1^+$ cells keeps getting progressively bigger from P5 until P30 (Fig. S3).

We also observed changes in the distribution of OD values depending on age (Fig. 2). At P5, $MSK1^+$ cells concentrate in low OD values, while at P10 they move to medium values, with few cells in either very low or very high OD. At P15 they go back to mainly low OD values, and at P30 the distribution gets more homogeneous, with cells in low, medium, and high OD (Fig. 2C). Together, these data show that *Msk1* expression is temporarily regulated during striatal development at two different stages, between P5 to P10 and between P15 to P30.

Generation and characterization of *Msk1 Exon IV* KO mice.

To understand the role of MSK1 during mouse brain development and adulthood, we generated a new *Msk1* knock-out model. For it, we removed the *Msk1* Exon IV with CRISPR/Cas9 to generate a premature STOP codon (TGA) in the Exon V (Fig. 3A and B). We targeted Exon IV, and not Exon I, due to the presence of an alternative ATG start codon in the Exon III of the gene that it is frame with the ORF and that could, putatively, be used as an alternative to the ATG located in EXON I were removed. We confirmed the edition by Sanger sequencing (Fig. 3A) and genotyped the offspring by two PCRs (Fig. 3C). The *Msk1 Exon IV* KO– *mice* ($Msk1^{IV}$ KO) are viable and fertile, with non-evident developmental problems or abnormalities at P30 such as different size or weight compared to control littermates, gross body tremors, hindlimb or forelimb clasping. We did not detect MSK1 protein levels by western blot (Fig. 3D) and immunofluorescence assays when using specific antibodies directed against the C-terminal domain (Fig. S4A).

Also, we found that *Msk1* transcript levels in these mice are significantly reduced compared to control mice (Fig. 3E), probably due to a nonsense-mediated RNA decay process derived from the gene editing (52).

MSK1 mediates postnatal striatal growth and MSNs arborization.

Using Cavalieri´s method, we found a significant difference in the volume of striatum between wild-type and *MSK1*^{IV} KO littermate mice at P60 (Fig 3F – 3I and Fig. S4). However, there is not a significant reduction in the total length and weight between the brains of the *MSK1*^{IV} KO and WT mice at this age (Fig. S4B). The arborization of cultured striatal neurons relies on the BDNF-dependent MAPK pathway activation (34). Therefore, we considered that MSK1 could mediate the growth of MSNs during mouse brain development in a cell autonomous way. To test this hypothesis, we transfected wild-type striatal cultured neurons with control or specific MSK1 miRNAs-based shRNAs (shMSK1) (Fig. S5). We found that the length, number of primary dendrites, and arbor complexity was reduced in the absence of MSK1, even under the presence of BDNF (Fig. 3J). Moreover, the total number of primary dendrites, neurite complexity and length were rescued by overexpression of a mutant form of MSK1 (mutMSK1) resistant to the shMSK1 (Fig. 3J). These results show that MSK1 controls the BDNF-dependent arborization of mouse striatal MSNs and is required for normal striatal maturation.

MSK1 mediates BDNF-dependent MeCP2 S421 phosphorylation.

Stimulation of cortical/hippocampal neurons with BDNF induces, besides gene transcription, phosphorylation of MeCP2 through the CaMKII pathway but independently of ERK1/2 (39). MeCP2 is expressed by both glutamatergic and GABAergic neurons, and its activity is critical for proper brain development and striatal function

(48). MSK1 substrates include several transcription factors such as CREB, Histone H3 and the DNA binding proteins of the high mobility group (HMG) (53, 54). We hypothesized that MSK1 could also mediates BDNF-dependent MeCP2 phosphorylation in striatal neurons. BDNF treatment led to, as previously reported (55), an increase in TrkB and ERK1/2 phosphorylation in cultured striatal neurons, but also to MeCP2 S421 phosphorylation (Fig. 4A). The latter was reduced after inhibiting the MAPK pathway with U0126 (FIG. 4A) and also by the absence of MSK1 (Fig. 4B). Next, we tested if MSK1 and MeCP2 interact in the cell nucleus. Western blotting of HA immunoprecipitates, obtained from purified nuclear lysates of HEK293 cells expressing HA-MeCP2 and MSK1-myc, shows that both proteins interact independently of their phosphorylation state (Fig. 4C). Together, these results suggest that MSK1 forms part of a nuclear complex with MeCP2, and that in striatal neurons MSK1 is required for the BDNF-dependent MeCP2 S421 phosphorylation.

Changes in the expression of genes related to the GABA and dopamine system in the *Msk1^{IV}* KO mice.

The lack of *Mecp2* in the striatum alters gene transcription (47, 48). To address whether the transcriptional effects of MeCP2 were dependent of MSK1 we decided to study, among others, the mRNA levels of genes which expression is altered by the lack of MeCP2 in the striatum. We found by qPCR of cDNAs obtained from the striata of P60 *Msk1^{IV}* KO mice, a reduction in the expression levels of the gene glutamate decarboxylase 1 (*Gad1*), which codes for GAD67, and an increment in the expression of the specific MSNs $GABA_A$ receptor subunit gamma 3 (*Gabrg3*), compared to those of wild type mice (Fig. 4D). Moreover, while the mRNA expression of the dopamine receptors *Drd1 and Drd3* was reduced, those for *Drd2* were significantly increase (Fig. 4E) (48, 56). Furthermore, we observed no changes in the expression of *Grin1a*, (N-Methyl-D-Aspartate Receptor Subunit NR1), *Psd95* (glutamatergic

post-synaptic density protein 95) and the serotonin receptor *5-Htr2c* (5-Hydroxytryptamine Receptor 2C) (Fig. S6). So, as for mice in which *Mecp2* is removed only in GABAergic neurons (47, 48), the lack of MSK1 in our mutant mice also affects the expression of the genes *Irak1* (Interleukin-1 receptor-associated kinase 1)*, Satb1* (special AT-rich sequence binding protein 1)*, Dlk1* (delta like non-canonical Notch ligand 1) *and Pvalb* (parvalbumin) (Fig. S6). On the contrary, we found no changes in neither the expression of the specific MSNs gene *Darpp-32* nor in the astrocytic gene *Gfap* (glial fibrillary acidic protein)*,* but a reduction in the levels of *Ppargc1a* (peroxisome proliferator-activated receptor gamma coactivator 1-alpha) (Fig. S6), whose expression is known to be dependent on MSK1 (49).

Altogether, our data indicate that MSK1 is required for the expression of genes implicated on the functionality of the GABA and dopamine networks in the striatum, in a similar way to what has been described for *Mecp2*-deficient mice.

Altered emotional behaviour in *Msk1^{IV}* KO mice.

To investigate the behavioural consequences, if any, in our KO mouse model, we first decided to test the locomotor activity of males and females by the open field and the accelerating rotarod assays (Fig. 5A and B). Surprisingly, we observed that *Msk1^{IV}* KO males, but not mutant females, entered more and spent longer time in the centre of the open field (Fig. 5A), suggesting an anxiety defect in males but not females. As this could be due to a possible emotional behavioural problem, we evaluated the innate and specific social responses together with anxious and depressive behaviours on both genders. We assessed innate responses by the nest building test, which has been shown to be dopamine-dependent (57), while used the three-chambered social test to analyse the specific social behaviour. When compared to control mice, both *Msk1^{IV}* KO males and females showed poorer nest building at 4h and 24h (Fig. 5C). In addition, both genders

showed hypersocial behaviours, as they spent longer time sniffing for a conspecific mouse than control wild-type mice in the three-chambered social test (Fig. 5D). When analysing the anxiety response by the marble-burying test, *Msk1*^{IV} KO males but not females buried less marbles than controls (Fig. 5E). Finally, we observed that *Msk1*^{IV} KO mice remained immobile for longer time than control littermates in the forced swimming test (FST), showing a depressive-like or demotivation behaviour (Fig. 5F). All together, these data indicate that the lack of MSK1 from embryogenesis alters adult mouse behaviour, causes hypersociability, depressive-like symptoms in both genders, but less responses to stimuli, such as the caused by the open field- and marble burying- test, that generate anxiety only in mutant male mice.

Discussion.

Our study uncovers a new molecular mechanism through which the lack of MSK1, which expression we found to be controlled during development in GABAergic neurons, impacts the arborization of MSNs and the growth of the striatum. This absence leads to the lack of phosphorylation of MeCP2, and results in the misregulation of genes related to GABAergic and dopamine responses in the adult mouse striatum. These abnormalities are linked to atypical innate and social responses, as well as anxiety and depression-like behaviours, in both male and female mice. Our findings support the notion that dysfunction in the striatum due to developmental abnormalities caused by the lack of MSK1, might play a central role in the pathophysiology of schizophrenia.

MSK1 expression is controlled during development.

It has been well studied that MSK1 expression in adult mouse brain is highest in striatal MSNs and Purkinje neurons in the cerebellum (49, 50, 58–60), but much lower in the brain cortex and hippocampus (50, 59). Our results demonstrate that MSK1 expression in the early postnatal somatosensory cortex and striatum is mainly restricted to

GABAergic neurons. Also, we observed that its expression is differentially regulated in both areas during postnatal development. While MSK1 expression decreases in the somatosensory cortex, striatal cells increase it. This reveals that both striatal and cortical GABAergic neurons respond differently to stimuli controlling MSK1-dependent neuronal regulation. However, it still remains unclear whether these stimuli control similar signalling pathways that leads to MSK1 activity in both neuronal populations.

MSK1 is primarily expressed by MSNs in the adult striatum (49). Due to this, the different MSNs populations, that differ in the expression of the dopaminergic receptors DRD1 or DRD2, should be the most affected by the lack of MSK1 during postnatal brain development. Of note, our morphometric and densitometric results indicate that MSK1 expression is not equal, neither constant, in all striatal cells during postnatal development. While this may indicate a different maturation stage of the various MSNs populations, it is also possible that the maturation of the dorsal and ventral striatum differs due to the regulation of different genes that depends on MSK1. More detailed experiments should be done in the future to test this hypothesis.

MSK1 role in postnatal maturation of striatum and arborization.

Many studies have described that BDNF controls axonal and dendritic arborization of neurons depending on their class (29, 30, 32, 33, 37, 61, 62). In terms of neuronal arborization, some reports have shown that pyramidal neurons located in layer IV are more responsive that those located in layer VI (32, 33). Others have shown that hippocampal glutamatergic neurons arbors, but not hippocampal GABAergic neurons, are almost unaltered by the presence of BDNF (29). Studies with mice lacking BDNF in the CNS revealed an area-specific requirement for dendritic growth of striatal neurons but not for the growth of CA1 pyramidal neurons, suggesting that the differential

responsiveness to BDNF depends on neuron-specific programs (30, 31).

The BDNF/ MAPK pathway is required for the proper growth of MSNs as well as for the postnatal growth of the striatum (30, 34, 63). BDNF mediates the activation of the RSK (RSK1, RSK2, RSK3 and RSK) and MSK (MSK1, MSK2) family members (64–66). Our data on MSK1 developmental expression in the striatum raise the possibility that it controls the specific growth of MSNs. Indeed, we observed that the lack of MSK1 clearly affects the postnatal growth of the striatum. Moreover, we found that the specific downregulation of MSK1 in striatal cultured neurons leads to a significant poor arborization even in the presence of BDNF. RSKs and MSKs can be activated by similar signals, suggesting some redundancy in the phosphorylation of substrates *in vitro*. However, some RSKs and MSK1 shown different cellular localization in the adult mouse brain (50, 58). Our results show postnatal regulated expression of MSK1 in GABAergic interneurons and MSNs and suggest that the functions of the RSK and MSK family members could not be totally redundant. Therefore, it would be interesting to compare the expression of the RSK and MSK proteins and their role during development in different neuronal types in order to confirm this hypothesis.

Altered gene expression and behavioural features in MSK1^{IV} knockout mice.

Our results demonstrate that MSK1 interacts and controls BDNF-dependent MeCP2 S421 phosphorylation in striatal neurons. These results seem to differ from those others that show that MAPK signalling does not mediate MeCP2 phosphorylation, but it is dependent on the activation of CaMKII by BDNF (39). Of note, MeCP2 is expressed not only by glutamatergic but also by GABAergic neurons in different brain areas. Therefore, we expect that the discrepancy between our results and the ones mentioned, could be due to the different type of neurons

that we are analysing, striatal neurons, instead the analysed in those studies, cortical/hippocampal neurons.

In our study, we found that ablation of MSK1 alters striatal expression of *Gad1*, *Drd1*, *Drd2*, *Drd3*, *Pvalb* and *Irak1*, similarly to what has been observed in mice lacking MeCP2 in GABAergic neurons (47, 67, 68). These data show that MSK1 influences the GABA and dopamine system in the striatum. However, the lack of alterations on the expression of *Psd95* and the serotonin receptor *5-Htrc-2* by the MSNs, indicates that MSK1 is not involved in the regulation of the glutamatergic afferent projections that receive these neurons from cortical areas, neither in the serotonin-dependent functions. MSK1 regulates gene expression by modulating the phosphorylation of Histone H3 (69), transcription factors such as CREB (70, 71), and DNA binding proteins (72, 73). Our experimental evidence suggests that MSK1-dependent MeCP2 S421 phosphorylation also modulates genes involved in GABA and dopamine functions in the striatum. Despite its role as regulator of MeCP2 activity, MSK1 depleted mice do not show Rett syndrome-like features but resemble some of the features observed in mice lacking MeCP2 expression in MSNs. At their core, behavioural dysfunctions observed in MeCP2 null mice will most likely be due to a combination of alterations of glutamatergic and GABAergic circuits in different brain areas including striatum.

Msk1^{IV} KO mice display some features linked to striatal and dopamine functions that are also observed in Schizophrenia patients (74). There are several mouse models where it has been shown that dysfunctions in the development of the GABAergic network (28) and the dopaminergic system (75) are implicated in Schizophrenia. The reduction in *Drd1* and increment on *Drd2* mRNA levels in our *Msk1*^{IV} KO mice, indicates a possible disruption on the dopamine signalling. MSNs constitute two different pathways that controls movement: the direct pathway, controlled by DRD1 expressing MSNs (D1-MSNs), implicated in movement promotion, and the indirect pathway,

controlled by DRD2-MSNs (D2-MSNs) inhibiting movement. Surprisingly, our mice do not show motor impairments, despite the degree of affectation in the mRNA levels of both dopamine receptors and the striatal growth. In a transgenic mouse model, it has been observed that overexpression of DRD2 results in hyperactivity, primarily caused by a reduced rate of dopamine reuptake in the synaptic space (76). It is important to note that the levels of DRD1 remain unaffected in these mice, indicating that high levels of DRD2 do not necessarily correlate with reduced expression levels of DRD1. It is possible that the imbalance in dopamine receptors expression observed in *Msk1*^{IV} KO mice could be a result of a compensatory mechanism without leading to alterations on the motor behaviour. Further studies on the activity and regulation of dopamine receptors should be done to investigate the mechanisms that enable normal movement in MSK1-deficient mice, despite the unbalanced expression of dopamine receptors in the striatum.

Similar to *Erbb4*-deleted and *Glud1*-deficient mice (28, 77), which are Schizophrenia-like mouse models, nesting behavior is disrupted in *Msk1*^{IV} KO mice. This suggests that our mice exhibit self-neglect attitudes, which is a characteristic of the negative symptoms observed in individuals with schizophrenia disorder (78). Other negative symptoms, such as depression, demotivation, and avolition, are typically assessed using the forced swimming test (FST) in mice (79). In this test, *Msk1*^{IV} KO mice display increased freezing time, indicating depressive and demotivated behavior. Additionally, we observed a lack of motivation in the marble burying test only in male *Msk1*^{IV} KO mice, as these bury a significantly lower number of marbles compared to control littermates, similarly to what was reported for male *Erbb4* mutant mice (28).

In addition, *Msk1*^{IV} KO mice are overly social compared to controls, as they spend more time interacting with conspecific. This is a characteristic of some neuropsychologic illness mouse models like

Grin1 KO*,* a schizophrenia-like mouse model (80). Hypersociability is related with a reduction in the source of BDNF from the Ventral Tegmental Area (VTA) to the Nucleus Accumbes (NAc), a major component of the ventral striatum involved in mediating motivational and emotional processes (81). The lack of MSK1 in the MSNs of the NAc could emulate the lack of BDNF arriving from the VTA, as we have observed in our striatal cultures. Due to this, MSK1 absence would lead to the hypersocial behavior observed in the *Msk1*^{IV} KO mice.

Our study reveals different behaviors between male and female *Msk1*^{IV} KO, reflected in both the frequency in entering to the center of the open field, as in the number of buried marbles. One explanation could be related to the dysregulated expression levels of dopamine receptors in MSN. It has been reported that the higher DRD1-DRD2 heteromers expression found in female rats, and that are regulated by the BDNF/TrkB pathway, may increase their predisposition to anxiety-like behavior (82). New studies on the regulation of DRD1 and DRD2 expression would address the mechanisms underlying the ability of MSK1 in regulating different sexual behaviors.

The effects of sex on schizophrenia are multifaceted and complex, encompassing variations in symptom manifestation, social outcomes, and responses to treatment between men and women. Understanding these differences is of utmost importance in order to develop more effective and personalized treatments for individuals living with schizophrenia. Hence, it is tempting to speculate that the severity of the behavioural phenotype displayed by MSK1 mutant mice depends on the development of neurons and brain regions where this gene is most highly expressed, namely the GABAergic network and areas modulated by the striatal projection neurons.

Our data highlights the view that MSK1 modulation may open new therapeutic approaches and provide mechanistic insights into the cell autonomous regulation of GABAergic axonal arborization, as well as

gene expression, and supports the role of pathological mutations in MSK1 that could lead to schizophrenia-like behaviours.

Methods

Animals.

All experiments using mice were conducted with permission from the Council of Agriculture and Livestock of Castilla y Leon Government, after approval by the ethical committee of the University of Salamanca and following the European Directive 2010/63/EU and the Spanish Royal Decree 53/2013-Law 32/2007. All animals were kept on a 12:12 light/dark cycle, receiving food and water *ad libitum*.

Quantitative Real-Time PCR (qPCR).

Specific and validated oligonucleotides for each analysed transcript were used. Relative expression levels were compared with TBP levels by the $2^{-(\Delta\Delta Ct)}$ method.

Quantitative Western Blot.

Total protein lysates were analysed in 10% Bis-Tris gels, transferred to Immobilon membranes (Merck) and incubated with specific primary antibodies against: MSK1 (Cell Signaling), β-actin (Proteintech), pTrkB (Cell Signaling), pERK1/2 (Cell Signaling), pMeCP2 (Abcam), Myc-tag (SantaCruz) and visualized using IRDye secondary antibodies (LI-COR). Fluorescent images were acquired using an Odyssey XF Imaging system. Data were analysed using the Empiria Studio™ Software.

Immunohistochemistry.

Brains were obtained from mice after intracardial perfusion with 4% PFA, cryoprotected and later sectioned using a cryotome (40 μm thickness/slice). Brain slices were analysed using primary monoclonal antibodies against MSK1 (Cell Signaling) and DARPP-32 (Santa Cruz), and visualized using AF488-, or AF555-conjugated secondary antibodies (ThermoFisher), or biotinylated secondary antibodies (Vector Labs). Nuclei were counterstained with Hoechst 33342 (4 μM,

Invitrogen). Fluorescent images were captured with a Leica Stellaris 8 confocal microscope. High-resolution microphotographs were taken under a Leica DMRX microscope to prepare whole-section digital mosaics.

Primary striatal cultures.

Embryonic day (E) 14.5-16.5 striatal neurons (3.0 x 10^5 cells/cm^2) were grown in supplemented Neurobasal medium (2% B27, 10mM HEPES, 0.2 mM glutamine, penicillin 10 μg/mL, streptomycin 10 μg/mL) on poly-D-lysine and laminin overnight coated plates and glass coverslips.

HEK293-FT cell cultures.

Cells were grown in supplemented DMEM medium (10 % FCS, 2mM glutamine, 10 mM HEPES, Penicillin 10 μg/mL, Streptomycin 10 μg/mL, 1% MEM non-essential amino acids, 0.001 % 2-mercaptoethanol).

Cell transfections.

Primary striatal cultures were transfected using FuGENE 6 (Promega). HEK293T cells were transfected using linear polyethylenimine (Polysciences).

$Msk1^{IV}$ KO mouse line generation.

One-cell C57BL/6J mouse zygotes were microinjected with Cas9/sgRNAs complexes to induce the excision of the Exon IV of *Msk1* gene. Offspring were analysed by Sanger sequencing to confirm the removal of the Exon IV. Founder animals (F0) were bred to C57Bl/6J wild-type mice.

Immunocytochemistry.

Fixed cells were processed using anti-EGFP antibodies (Cell Signaling) and visualized with AF488 conjugated secondary antibodies (ThermoFisher).

Striatal volumetric analysis.

Each brain was totally sectioned using a cryotome (40μm thickness) and divided in 10 consecutive series. Total striatal volume was assayed using Cavalieri´s mathematical formula.

Neuronal morphology analysis.

Transfected neurons expressing EGFP were visualized using standard epifluorescence under a 5x Neofluar objective. Sholl analyses were performed with the help of the ImageJ software.

Behavioural tests.

The experiments were performed on 2 to 4 months old male and female mice from 10 different cohorts. All behavioural experiments were performed in a randomized manner.

Statistical analysis.

All statistical tests were performed using GraphPad Prism 8.0.1. Any result with a *P* value <0.05 was considered statistically significant.

A full description of all methods can be found in SI Appendix.

Acknowledgments.

We thank Prof. Yves-Alain Barde for discussions and ideas during the initial steps of this study, Prof. Alberto M. Pendás and members of the M.M., J.C.A. and R.D. laboratories for stimulating discussions and ideas. This work was supported by grants from the Spanish Ministry of Science and Innovation to R.D. (RYC2018/205215-I, PID2020-113086RB-I00 and CNS2022-136048) and M.M (PID2020-117266RB-C21). N.V-A. has a contract from the University of Salamanca / Banco Santander. A. C-L, C.H-C and S.G-L contracts are associated to PID2020-113086RB-I00 and CNS2022-136048 grants. USAL/IBSAL Transgenic Facility, directed by M.S-M, are supported by Instituto de Salud Carlos III (ISCIII), co-funded by the European Union grant PT23/00123 to M.S.M.

Author contributions.

Conceptualization: R.D.; Investigation: R.D., N.V-A., A.C-L., C.H-C., I.S.F-C., S.G-L., N.M-A.; Methodology: R.D., M.S-M., M.M., J.C.A.; Formal Analysis: R.D., N.V-A., A.C-L., C.H-C., I.S.F-C.; Data curation: R.D., M.M.; Writing – original draft preparation: R.D., N.V-A., A.C-L., C.H-C., I.S.F-C.; Writing – review and editing: All authors; Supervision: R.D.

References

1. Z. J. Huang, *et al.*, BDNF regulates the maturation of inhibition and the critical period of plasticity in mouse visual cortex. *Cell* **98**, 739–755 (1999).

2. E. J. Hong, A. E. McCord, M. E. Greenberg, A biological function for the neuronal activity-dependent component of Bdnf transcription in the development of cortical inhibition. *Neuron* **60**, 610–624 (2008).

3. C. Sánchez-Huertas, B. Rico, CREB-Dependent Regulation of GAD65 Transcription by BDNF/TrkB in Cortical Interneurons. *Cereb Cortex* **21**, 777–788 (2011).

4. K. Zheng, *et al.*, TrkB signaling in parvalbumin-positive interneurons is critical for gamma-band network synchronization in hippocampus. *Proc Natl Acad Sci U S A* **108**, 17201–17206 (2011).

5. E. G. Waterhouse, *et al.*, BDNF promotes differentiation and maturation of adult-born neurons through GABAergic transmission. *J Neurosci* **32**, 14318–14330 (2012).

6. E. Cherubini, J. L. Gaiarsa, Y. Ben-Ari, GABA: an excitatory transmitter in early postnatal life. *Trends in Neurosciences* **14**, 515–519 (1991).

7. S. Bolea, E. Avignone, N. Berretta, J. V. Sanchez-Andres, E. Cherubini, Glutamate controls the induction of GABA-mediated giant depolarizing potentials through AMPA receptors in neonatal rat hippocampal slices. *J Neurophysiol* **81**, 2095–2102 (1999).

8. T. N. Behar, *et al.*, GABA(B) receptors mediate motility signals for migrating embryonic cortical cells. *Cereb Cortex* **11**, 744–753 (2001).

9. G. López-Bendito, *et al.*, Blockade of GABAB Receptors Alters the Tangential Migration of Cortical Neurons. *Cerebral Cortex* **13**, 932–942 (2003).

10. K. M. Money, G. D. Stanwood, Developmental origins of brain disorders: roles for dopamine. *Front Cell Neurosci* **7**, 260 (2013).

11. R. Z. Chen, S. Akbarian, M. Tudor, R. Jaenisch, Deficiency of methyl-CpG binding protein-2 in CNS neurons results in a Rett-like phenotype in mice. *Nat Genet* **27**, 327–331 (2001).

12. J. Guy, B. Hendrich, M. Holmes, J. E. Martin, A. Bird, A mouse Mecp2-null mutation causes neurological symptoms that mimic Rett syndrome. *Nat Genet* **27**, 322–326 (2001).

13. M. D. Shahbazian, B. Antalffy, D. L. Armstrong, H. Y. Zoghbi, Insight into Rett syndrome: MeCP2 levels display tissue- and cell-specific differences and correlate with neuronal maturation. *Hum Mol Genet* **11**, 115–124 (2002).

14. L. Caracciolo, *et al.*, CREB controls cortical circuit plasticity and functional recovery after stroke. *Nat Commun* **9**, 2250 (2018).

15. E. J. Hong, A. E. West, M. E. Greenberg, Transcriptional control of cognitive development. *Curr Opin Neurobiol* **15**, 21–28 (2005).

16. T. A. Pham, J. L. Rubenstein, A. J. Silva, D. R. Storm, M. P. Stryker, The CRE/CREB pathway is transiently expressed in thalamic circuit development and contributes to refinement of retinogeniculate axons. *Neuron* **31**, 409–420 (2001).

17. W. Li, L. Pozzo-Miller, BDNF deregulation in Rett syndrome. *Neuropharmacology* **76 Pt C**, 737–746 (2014).

18. V. R. B. Liyanage, M. Rastegar, Rett syndrome and MeCP2. *Neuromolecular Med* **16**, 231–264 (2014).

19. E. H. Simpson, C. Kellendonk, E. Kandel, A Possible Role for the Striatum in the Pathogenesis of the Cognitive Symptoms of Schizophrenia. *Neuron* **65**, 585–596 (2010).

20. T. J. Brozoski, R. M. Brown, H. E. Rosvold, P. S. Goldman, Cognitive deficit caused by regional depletion of dopamine in prefrontal cortex of rhesus monkey. *Science* **205**, 929–932 (1979).

21. T. Hashimoto, D. A. Lewis, BDNF Val66Met polymorphism and GAD67 mRNA expression in the prefrontal cortex of subjects with schizophrenia. *Am J Psychiatry* **163**, 534–537 (2006).

22. T. D. Purves-Tyson, A. M. Brown, C. Weissleder, D. A. Rothmond, C. Shannon Weickert, Reductions in midbrain GABAergic and dopamine neuron markers are linked in schizophrenia. *Molecular Brain* **14**, 96 (2021).

23. E. F. Osimo, K. Beck, T. Reis Marques, O. D. Howes, Synaptic loss in schizophrenia: a meta-analysis and systematic review of synaptic protein and mRNA measures. *Mol Psychiatry* **24**, 549–561 (2019).

24. T. U. Woo, J. L. Miller, D. A. Lewis, Schizophrenia and the parvalbumin-containing class of cortical local circuit neurons. *Am J Psychiatry* **154**, 1013–1015 (1997).

25. N. C. Allen, *et al.*, Systematic meta-analyses and field synopsis of genetic association studies in schizophrenia: the SzGene database. *Nat Genet* **40**, 827–834 (2008).

26. J. G. Mulle, Schizophrenia genetics: progress, at last. *Curr Opin Genet Dev* **22**, 238–244 (2012).

27. E. M. Sullivan, P. O'Donnell, Inhibitory interneurons, oxidative stress, and schizophrenia. *Schizophr Bull* **38**, 373–376 (2012).

28. I. Del Pino, *et al.*, Erbb4 deletion from fast-spiking interneurons causes schizophrenia-like phenotypes. *Neuron* **79**, 1152–1168 (2013).

29. C. Vicario-Abejón, C. Collin, R. D. McKay, M. Segal, Neurotrophins induce formation of functional excitatory and inhibitory synapses between cultured hippocampal neurons. *J Neurosci* **18**, 7256–7271 (1998).

30. S. Rauskolb, *et al.*, Global deprivation of brain-derived neurotrophic factor in the CNS reveals an area-specific requirement for dendritic growth. *J Neurosci* **30**, 1739–1749 (2010).

31. J. A. Gorski, S. R. Zeiler, S. Tamowski, K. R. Jones, Brain-derived neurotrophic factor is required for the maintenance of cortical dendrites. *J Neurosci* **23**, 6856–6865 (2003).

32. A. K. McAllister, L. C. Katz, D. C. Lo, Opposing Roles for Endogenous BDNF and NT-3 in Regulating Cortical Dendritic Growth. *Neuron* **18**, 767–778 (1997).

33. A. K. McAllister, D. C. Lo, L. C. Katz, Neurotrophins regulate dendritic growth in developing visual cortex. *Neuron* **15**, 791–803 (1995).

34. N. Gavaldà, E. Pérez-Navarro, E. Gratacòs, J. X. Comella, J. Alberch, Differential involvement of phosphatidylinositol 3-kinase and p42/p44 mitogen activated protein kinase pathways in brain-derived neurotrophic factor-induced trophic effects on cultured striatal neurons. *Mol Cell Neurosci* **25**, 460–468 (2004).

35. A. Barco, *et al.*, Gene expression profiling of facilitated L-LTP in VP16-CREB mice reveals that BDNF is critical for the maintenance of LTP and its synaptic capture. *Neuron* **48**, 123–137 (2005).

36. S. Finkbeiner, *et al.*, CREB: A Major Mediator of Neuronal Neurotrophin Responses. *Neuron* **19**, 1031–1047 (1997).

37. G. Moya-Alvarado, *et al.*, BDNF/TrkB signaling endosomes in axons coordinate CREB/mTOR activation and protein synthesis in the cell body to induce dendritic growth in cortical neurons. *Elife* **12**, e77455 (2023).

38. J. Xing, J. Kornhauser, Z. Xia, E. Thiele, M. Greenberg, Nerve Growth Factor Activates Extracellular Signal-Regulated Kinase and p38 Mitogen-Activated Protein Kinase Pathways To Stimulate CREB Serine 133 Phosphorylation. *Molecular and cellular biology* **18**, 1946–55 (1998).

39. Z. Zhou, *et al.*, Brain-Specific Phosphorylation of MeCP2 Regulates Activity-Dependent Bdnf Transcription, Dendritic Growth, and Spine Maturation. *Neuron* **52**, 255–269 (2006).

40. B. Pérez-Cadahía, *et al.*, Role of MSK1 in the Malignant Phenotype of Ras-transformed Mouse Fibroblasts*. *Journal of Biological Chemistry* **286**, 42–49 (2011).

41. G. R. Wiggin, *et al.*, MSK1 and MSK2 are required for the mitogen- and stress-induced phosphorylation of CREB and ATF1 in fibroblasts. *Mol Cell Biol* **22**, 2871–2881 (2002).

42. L. Privitera, *et al.*, Experience Recruits MSK1 to Expand the Dynamic Range of Synapses and Enhance Cognition. *J Neurosci* **40**, 4644–4660 (2020).

43. S. A. L. Corrêa, *et al.*, MSK1 regulates homeostatic and experience-dependent synaptic plasticity. *J Neurosci* **32**, 13039–13051 (2012).

44. K. M. S. E. Reyskens, J. S. C. Arthur, Emerging Roles of the Mitogen and Stress Activated Kinases MSK1 and MSK2. *Front Cell Dev Biol* **4**, 56 (2016).

45. K. Brami-Cherrier, *et al.*, Parsing Molecular and Behavioral Effects of Cocaine in Mitogen- and Stress-Activated Protein Kinase-1-Deficient Mice. *J Neurosci* **25**, 11444–11454 (2005).

46. T. Hashimoto, *et al.*, Relationship of brain-derived neurotrophic factor and its receptor TrkB to altered inhibitory prefrontal circuitry in schizophrenia. *J Neurosci* **25**, 372–383 (2005).

47. K. Ure, *et al.*, Restoration of Mecp2 expression in GABAergic neurons is sufficient to rescue multiple disease features in a mouse model of Rett syndrome. *Elife* **5**, e14198 (2016).

48. Y.-T. Zhao, D. Goffin, B. S. Johnson, Z. Zhou, Loss of MeCP2 function is associated with distinct gene expression changes in the striatum. *Neurobiol Dis* **59**, 257–266 (2013).

49. E. Martin, *et al.*, Mitogen- and stress-activated protein kinase 1-induced neuroprotection in Huntington's disease: role on chromatin remodeling at the PGC-1-alpha promoter. *Hum Mol Genet* **20**, 2422–2434 (2011).

50. D. Heffron, J. W. Mandell, Differential localization of MAPK-activated protein kinases RSK1 and MSK1 in mouse brain. *Brain Res Mol Brain Res* **136**, 134–141 (2005).

51. V. G. Carmona-Barrón, *et al.*, Comparing the effects of transcranial alternating current and temporal interference (tTIS) electric stimulation through whole-brain mapping of c-Fos immunoreactivity. *Front Neuroanat* **17**, 1128193 (2023).

52. A. Nickless, J. M. Bailis, Z. You, Control of gene expression through the nonsense-mediated RNA decay pathway. *Cell Biosci* **7**, 26 (2017).

53. H. Sattarifard, A. Safaei, E. Khazeeva, M. Rastegar, J. R. Davie, Mitogen- and stress-activated protein kinase (MSK1/2) regulated gene expression in normal and disease states. *Biochem Cell Biol* **101**, 204–219 (2023).

54. S. Thomson, *et al.*, The nucleosomal response associated with immediate-early gene induction is mediated via alternative MAP kinase cascades: MSK1 as a potential histone H3/HMG-14 kinase. *EMBO J* **18**, 4779–4793 (1999).

55. R. A. Segal, M. E. Greenberg, Intracellular signaling pathways activated by neurotrophic factors. *Annu Rev Neurosci* **19**, 463–489 (1996).

56. C. Chiron, *et al.*, Dopaminergic D2 receptor SPECT imaging in Rett syndrome: increase of specific binding in striatum. *J Nucl Med* **34**, 1717–1721 (1993).

57. T. N. Sager, *et al.*, Nest building performance following MPTP toxicity in mice. *Behav Brain Res* **208**, 444–449 (2010).

58. W.-S. Lee, *et al.*, Dual targeting of brain region-specific kinases potentiates neurological rescue in Spinocerebellar ataxia type 1. *EMBO J* **40**, e106106 (2021).

59. Y.-S. Choi, *et al.*, Mitogen- and Stress-Activated Protein Kinase 1 Regulates Status Epilepticus-Evoked Cell Death in the Hippocampus. *ASN Neuro* **9**, 1759091417726607 (2017).

60. W. B. Chwang, J. S. Arthur, A. Schumacher, J. D. Sweatt, The nuclear kinase mitogen- and stress-activated protein kinase 1 regulates hippocampal chromatin remodeling in memory formation. *J Neurosci* **27**, 12732–12742 (2007).

61. Z. C. Baquet, J. A. Gorski, K. R. Jones, Early Striatal Dendrite Deficits followed by Neuron Loss with Advanced Age in the Absence of Anterograde Cortical Brain-Derived Neurotrophic Factor. *J. Neurosci.* **24**, 4250–4258 (2004).

62. C. Martín-Rodríguez, *et al.*, TrkB deubiquitylation by USP8 regulates receptor levels and BDNF-dependent neuronal differentiation. *J Cell Sci* **133**, jcs247841 (2020).

63. Y. Li, *et al.*, Conditional ablation of brain-derived neurotrophic factor-TrkB signaling impairs striatal neuron development. *Proceedings of the National Academy of Sciences* **109**, 15491–15496 (2012).

64. H. Dudek, *et al.*, Regulation of neuronal survival by the serine-threonine protein kinase Akt. *Science* **275**, 661–665 (1997).

65. A. Bonni, *et al.*, Cell survival promoted by the Ras-MAPK signaling pathway by transcription-dependent and -independent mechanisms. *Science* **286**, 1358–1362 (1999).

66. J. S. C. Arthur, *et al.*, Mitogen- and stress-activated protein kinase 1 mediates cAMP response element-binding protein phosphorylation and activation by neurotrophins. *J Neurosci* **24**, 4324–4332 (2004).

67. H.-T. Chao, *et al.*, Dysfunction in GABA signalling mediates autism-like stereotypies and Rett syndrome phenotypes. *Nature* **468**, 263–269 (2010).

68. F.-C. Kao, S.-H. Su, G. C. Carlson, W. Liao, MeCP2-mediated alterations of striatal features accompany psychomotor deficits in a mouse model of Rett syndrome. *Brain Struct Funct* **220**, 419–434 (2015).

69. J. S. C. Arthur, MSK activation and physiological roles. *Front Biosci* **13**, 5866–5879 (2008).

70. S. Daumas, *et al.*, The Kinase Function of MSK1 Regulates BDNF Signaling to CREB and Basal Synaptic Transmission, But Is Not Required for Hippocampal Long-Term Potentiation or Spatial Memory. *eNeuro* **4**, ENEURO.0212-16.2017 (2017).

71. I. M. E. Beck, *et al.*, Altered subcellular distribution of MSK1 induced by glucocorticoids contributes to NF-kappaB inhibition. *EMBO J* **27**, 1682–1693 (2008).

72. R. K. McGinty, S. Tan, Principles of nucleosome recognition by chromatin factors and enzymes. *Curr Opin Struct Biol* **71**, 16–26 (2021).

73. Y. V. Postnikov, G. I. Belova, J.-H. Lim, M. Bustin, Chromosomal protein HMGN1 modulates the phosphorylation of serine 1 in histone H2A. *Biochemistry* **45**, 15092–15099 (2006).

74. R. A. McCutcheon, A. Abi-Dargham, O. D. Howes, Schizophrenia, Dopamine and the Striatum: From Biology to Symptoms. *Trends in Neurosciences* **42**, 205–220 (2019).

75. M. Toda, A. Abi-Dargham, Dopamine hypothesis of schizophrenia: Making sense of it all. *Curr Psychiatry Rep* **9**, 329–336 (2007).

76. P. F. Kramer, *et al.*, Dopamine D2 receptor overexpression alters behavior and physiology in Drd2-EGFP mice. *J Neurosci* **31**, 126–132 (2011).

77. S. S. Lander, *et al.*, Glutamate Dehydrogenase-Deficient Mice Display Schizophrenia-Like Behavioral Abnormalities and CA1-Specific Hippocampal Dysfunction. *Schizophr Bull* **45**, 127–137 (2019).

78. S. J. Barry, T. M. Gaughan, R. Hunter, Schizophrenia. *BMJ Clin Evid* **2012**, 1007 (2012).

79. M. J. Ang, S. Lee, J.-C. Kim, S.-H. Kim, C. Moon, Behavioral Tasks Evaluating Schizophrenia-like Symptoms in Animal Models: A Recent Update. *Curr Neuropharmacol* **19**, 641–664 (2021).

80. S. S. Moy, V. D. Nikolova, N. V. Riddick, L. K. Baker, B. H. Koller, Preweaning sensorimotor deficits and adolescent hypersociability in Grin1 knockdown mice. *Dev Neurosci* **34**, 159–173 (2012).

81. S. Salgado, M. G. Kaplitt, The Nucleus Accumbens: A Comprehensive Review. *Stereotact Funct Neurosurg* **93**, 75–93 (2015).

82. A. Hasbi, *et al.*, Sex difference in dopamine D1-D2 receptor complex expression and signaling affects depression- and anxiety-like behaviors. *Biol Sex Differ* **11**, 8 (2020).

83. S. Gascón, J. A. Paez-Gomez, M. Díaz-Guerra, P. Scheiffele, F. G. Scholl, Dual-promoter lentiviral vectors for constitutive and regulated gene expression in neurons. *J Neurosci Methods* **168**, 104–112 (2008).

84. R. Deogracias, *et al.*, Fingolimod, a sphingosine-1 phosphate receptor modulator, increases BDNF levels and improves symptoms of a mouse model of Rett syndrome. *Proc Natl Acad Sci U S A* **109**, 14230–14235 (2012).

Figure Legends

Figure 1. Differential expression of MSK1 during postnatal mouse brain development in cortex and striatum. (A) *Msk1* mRNA expression levels (qPCR) in cortex and striatum at different postnatal ages (P5, P10, P15 and P30). **P*<0.05, ***P*<0,01, ****P*<0.001 (mean ± SEM; n=3 animal/age group; Ordinary one-way ANOVA). (B) MSK1 expression levels (WB) in cortex and striatum at different postnatal ages using specific antibodies against the C-terminal domain of MSK1. **P*<0.05 (mean ± SEM; n=3 animals/age group; Ordinary one-way ANOVA). (C and F) Representative single plane

confocal images of MSK1 expression pattern (green) in the somatosensory cortex and striatum of 5- and 30-day-old *Vgat-IRES-CRE; Ai9-RLC*^{tdTomato} mice. Endogenous tdTomato fluorescence (red) reveals GABAergic neurons. Arrows point to cells co-expressing MSK1 and tdTomato. (D and E) Quantification of MSK1^{+} /tdTomato^{+} cells and tdTomato^{+}/MSK1^{+} cells in the somatosensory cortex at different postnatal ages. *P<0.05, **P<0.01, ***P<0.001 (mean ± SEM; n=3 mice/age group, 6-8 images per animal; Ordinary one-way ANOVA). (G and H) Quantification of MSK1^{+} cells and tdTomato^{+} MSK1^{+} cells in the striatum at different postnatal ages. **P<0.01 (mean ± SEM; n=3 mice, 6-8 images per animal; Ordinary one-way ANOVA). Scale bars = 100μm.

Figure 2. Developmental changes in MSK1^{+} cells in the mouse striatum. (A) IHC/DAB images showing MSK1^{+} cells in the brain at different stages of development (P5, P10, P15 and P30). (B) MATLAB maps showing the distribution and area of MSK1^{+} cells in the striatum at different postnatal ages (P5, P10, P15 and P30). Cells from the striatum have been highlighted and show variations in OD. (C) Distribution of OD values (blue – low OD, red – high OD) from striatal MSK1^{+} cells.

Figure 3 MSK1 controls postnatal striatal growth and arborization of striatal neurons. (A) *Msk1* Exon IV KO allele removal induced by CRISPR/Cas9 (top), and genomic Sanger sequencing (bottom) of the CRISPR/Cas9 edition result. (B) Exon IV removal creates a premature stop codon in Exon V, generating *Msk1*^{IV} KO mice. (C) PCR and scheme of the genotyping of *Msk1*^{IV} KO offspring using 2 different sets of primers (102/103 and 114/115). (D) Western Blot from cortical and striatal lysates of *Msk1*^{IV} KO mice shows total absence of MSK1 when using specific monoclonal antibodies against the C-terminal domain of MSK1. (E) Quantitative PCR shows that *Msk1* transcripts are significantly reduced from mRNA extracted from the

striatum of P30 *Msk1*^{IV} KO mice. ***P<0.01* (mean ± SEM; n=3; two tailed unpaired Student´s t test). (F and H) Representative coronal sections of wild-type and *Msk1*^{IV} KO mice immunostained for DARPP-32 at postnatal ages P30 and P60. Dashes lines indicate the boundary of the striatum, determined with the Allen Brain Atlas, considering both staining and the anatomical boundaries of the striatum. STR=Striatum, LV=Lateral Ventricle, HY=Hypothalamus, SI=Substantia Innominata, PIR=Piriform Cortex, cc=Corpus Callosum. Scale bars, 1mm. (G and I) Striatal volume estimation of *Msk1*^{IV} KO compared to wild-type mice at P30 and P60 applying Cavalieri´s principle. *P<0.05 (mean ± SEM; n=3 mice, 10 to 12 sections per brain; two tailed unpaired Student´s t test). (J) Representative images of 7 DIV cultured wild-type striatal neurons 5 days after transfection with a reporter plasmid for EGFP containing a control shRNA (shControl), shRNAs against MSK1 (shMSK1) or shRNAs against MSK1 plus a resistant form of MSK1 against them (shMSK1+mutMSK1). BDNF (50 ng/ml) was added 2 days after transfection. The reduced arborization caused by the shMSK1 even in the presence of BDNF is reversed by overexpression of mutMSK1. (K to N) EGFP positive neurons were analysed by fluorescence microscopy and neuronal arborization was quantified using Sholl analysis. *P<0.05, **P<0.01, ***P<0.001. (mean ± SEM; n=14 neurons per condition. Two-way ANOVA followed by Tukey´s multiple comparisons test).

FIGURE 4. MSK1 interacts and mediates BDNF-dependent MeCP2 S421 phosphorylation. (A and B) Quantitative Western-Blot analysis of WT and *Msk1*^{IV} KO cultured striatal neurons. (A) 1h BDNF (50 ng/mL) stimulation causes an increase in TrkB, ERK1/2 and MeCP2 S421 phosphorylation in WT cultured striatal neurons. ERK1/2 inhibition with U0126 prevents MeCP2 S421 phosphorylation. *P<0.05, **P<0.01 (mean ± SEM; n=3; two tailed unpaired Student´s t test). (B) The absence of MSK1 prevents the BDNF-dependent MeCP2 S421

phosphorylation in cultured *Msk1*^{IV} KO striatal neurons, but not the phosphorylation of TrkB and ERK1/2. *P<0.05, **P<0.01 (mean ± SEM; n=4; two tailed unpaired Student´s t test). (C) MSK1 and MeCP2 interact in the nucleus of HEK293-FT independently of MSK1 phosphorylation state. Lysates from HEK293-FT cells co-transfected with expression plasmids for MeCP2-HA and MSK1-myc were immunoprecipitated with anti-HA antibodies coupled to magnetic beads and western blots were performed to detect the interaction of MSK1 with MeCP2 before or after inducing MSK1 activation by PMA (200 nM; 1h). (D) Expression of MeCP2-regulated genes is also dependent of MSK1. qPCR analysis show downregulation of *Gad1*, responsible of GABA production, *Drd1* and *Drd3*, which code for dopamine receptors, in the striatum of P60 *Msk1*^{IV} KO mice. However, transcript levels for the gene coding the $GABA_A$ receptor subunit gamma3 (*Gabrg3*) and the dopamine receptor *Drd2* are increased. *P<0.05, ***P<0.001 (mean ± SEM; n=3; two tailed unpaired Student´s t test).

Figure 5. MSK1 deletion causes altered emotional behaviour. (A and B) Locomotor activity of adult *Msk1*^{IV} KO mice compared to control wild-type mice. (A) *Msk1*^{IV} KO mice do not show altered locomotor activity as determined by the Open Field Test. However, male mutant mice, but not females, enter more into the centre of the field and spend more time in the centre zone. (B) Rotarod test shows no motor impairment in *Msk1*^{IV} KO mice, independently of their sex. (C) Representative pictures of a nest built after 24h. Innate responses analysed by the nest building test at 4h and 24h in control and mutant male and female mice show that mutant mice have an inability to build a proper nest. (D) Three-chamber test assesses social behaviour of mutant males and females compared to their corresponding wild-type control. Mutant mice spend more time interacting with an unfamiliar conspecific mouse (sociability) or novel object (novelty) than control mice. (E) Analysis of the anxiety response assessed by the marble

burying test performed during 30min. *Msk1*^{IV} KO mice buried significantly less marbles than their wild-type littermates. No differences were observed between wild-type and mutant females. (F) Depressive-like state was analysed by the immobility time of mice during the Forced swimming test. Both male and mutant females show an increased immobility during the test compared to control mice. In all cases animals were 2 to 4 months old and statistical analysis was performed with two tailed unpaired Student´s t test *P<0.05, **P<0.01, ***P<0.001. (mean ± SEM; n= 9 to 13 mice per condition and sex).

Supplementary Figure Legends

Figure S1. MSK1 expression and distribution pattern change during postnatal brain development. Representative single plane confocal images of P5 to P30 barrel field area of the somatosensory cortex (SSp-bfd) of the *Vgat-IRES-CRE; Ai9-RLC*^{tdTomato} mice stained with specific anti-MSK1 antibodies. Note that endogenous expression of the fluorescent reporter tdTomato labels the soma and neurites of all interneurons in the area. Note the intense staining of the MSK1^{+} cells at P5 and how it decreases during development as well as the number of MSK1^{+} cells. Arrows point to tdTomato^{+} cells that are expressing MSK1.

Figure S2. Detection of MSK1 expression pattern in GABAergic neurons in the striatum during mouse brain development. Representative single plane confocal images of MSK1 expression in the striatum from P5 to P30 in mice expressing the reporter fluorescence protein tdTomato in GABAergic neurons. Note the dense neuronal network in the striatum during all the developmental stages and how the density of nuclei decreases with development but not MSK1 intensity. Arrows point to tdTomato^{+} cells that are expressing MSK1.

Figure S3. MSK1 expression in striatal neurons development. Statistical analysis of developmental changes in number, O.D. and size of MSK1$^+$ cells in the striatum. *P<0.05, **P<0.01, ***P<0.001. (mean ± SEM; n=3. Non-parametric Kruskal-Walli's test followed by *post hoc* Bonferroni test) (A) At P30 and P15 there is a significantly higher number of MSK1$^+$ cells than at P5 (P15 – P<0.001; P30 – P<0.000). (B) At P10 and P30, the OD of MSK1$^+$ cells is significantly higher than at P5 (**P<0.01, ***P<0.001)). (C) The area of MSK1$^+$ cells increases through development (**P<0.01, ***P<0.001).

Figure S4. Striatal volume is reduced in the *Msk1^{IV}* KO mice. (A) Low power magnification of coronal sections (medial: Bregma ≈ +0.045 mm) from P60 wild type and *Msk1^{IV}* KO mice stained with anti-MSK1 antibodies (green) and DARPP-32 (red). Note the intense staining for MSK1 in the striatum in the wild type and lack of immunoreactivity in the section of the mutant mouse. (B) Examples of a brain of a wild type and a *Msk1^{IV}*KO mice at 2 months old after PFA intracardial perfusion. No differences in length and weight were found in mutant brains compared to wild type brains. (mean ± SEM; n=5 wild type mice and n=3 *Msk1^{IV}* KO mice. two tailed unpaired Student´s t test). (C) Representative images of coronal sections (rostral: Bregma ≈ +1.42 mm, medial: Bregma ≈ +0.045 mm and caudal: Bregma ≈ -1.055 mm) of wild type and *Msk1^{IV}* KO mice immunostained for DARPP-32 and used for further striatal volume determination applying Cavalieri´s principle, using the Allen Brain Atlas and considering both staining and the anatomical boundaries of the striatum. (Scale bar in all images is 1mm). STR=striatum; LV=Lateral Ventricle, LS=Lateral Septum, SI=Substantia Innominata, EP=Endopiriform Cortex, HY=Hypothalamus, PIR=Piriform Cortex, cc=Corpus Callosum, int=Internal Capsule, GP=Globus Palidus, AMY=Amygdala.

Figure S5. Validation of human synapsin-promoter expression vectors containing miRNA-based shRNAs and a resistant form

of MSK1 (mutMSK1). (A) Scheme of the expression vectors for individual miRNA-based shRNAs. Control miRNA-based shRNA (shControl) against β-galactosidase. pLL-shM # (shM1, shM2, shM3 and shM4) are miRNA-based shRNAs against different regions of MSK1. The plasmid pLL-shMSK1 contains a cassette with the four miRNA-based shRNAs against MSK1. The expression vector pLL-mutMSK1 is a dual human synapsin-promoter vector allowing the independent expression of the fluorescent reporter protein DsRED and the protein MSK1 containing point mutations in its nucleotide sequence that confer resistant to the miRNA-based shMSK1-induced degradation. The vector pLL-shMSK1-mutMSK1 allows the expression of the cassette containing the four miRNA-based shRNAs against MSK1, the resistant form of MSK1 and the reporter fluorescent protein EGFP under the control of the promoters human synapsin. (B) Sequences of the miRNA-based shRNAs against MSK1 and the corresponding point mutations that change the nucleotide sequence but not the aminoacidic sequence to mutMSK1. (C) Western Blot showing the efficiency of each miRNA-based shRNA on HEK293-FT cells co-transfected with an expression plasmid for the murine wild-type MSK1 protein containing a myc-tag domain at the end of the 3´CDS. Note that the plasmid containing the cassette with the four miRNA-based shRNAs against MSK1 show a greater efficiency in downregulating MSK1 compared to the single miRNA-based shRNAs against MSK1. The construct expressing the shControl does not causes the reduction of the levels of MSK1myc.

Figure S6. Lack of MSK1 causes gene disregulation in the striatum. Transcript levels for different genes were analysed by qPCR using specific primers. No differences were observed in the expression of *Grin1a*, (N-Methyl-D-Aspartate Receptor Subunit NR1), *Psd95* (glutamatergic post-synaptic density protein 95) and the serotonin receptor 5-Htr2c (5-Hydroxytryptamine Receptor 2C), neither in the expression of *Darpp-32* and the astrocytic marker *Gfap*. We detected a

significant increase in the transcription for the genes *Irak1*, *Satb1*, *Dlk1* and *Pvalb*. We found a reduction on the transcription of the gene *Pgc1a*. * $P < 0.05$. (mean ± SEM; n=3; two tailed unpaired Student´s t test).

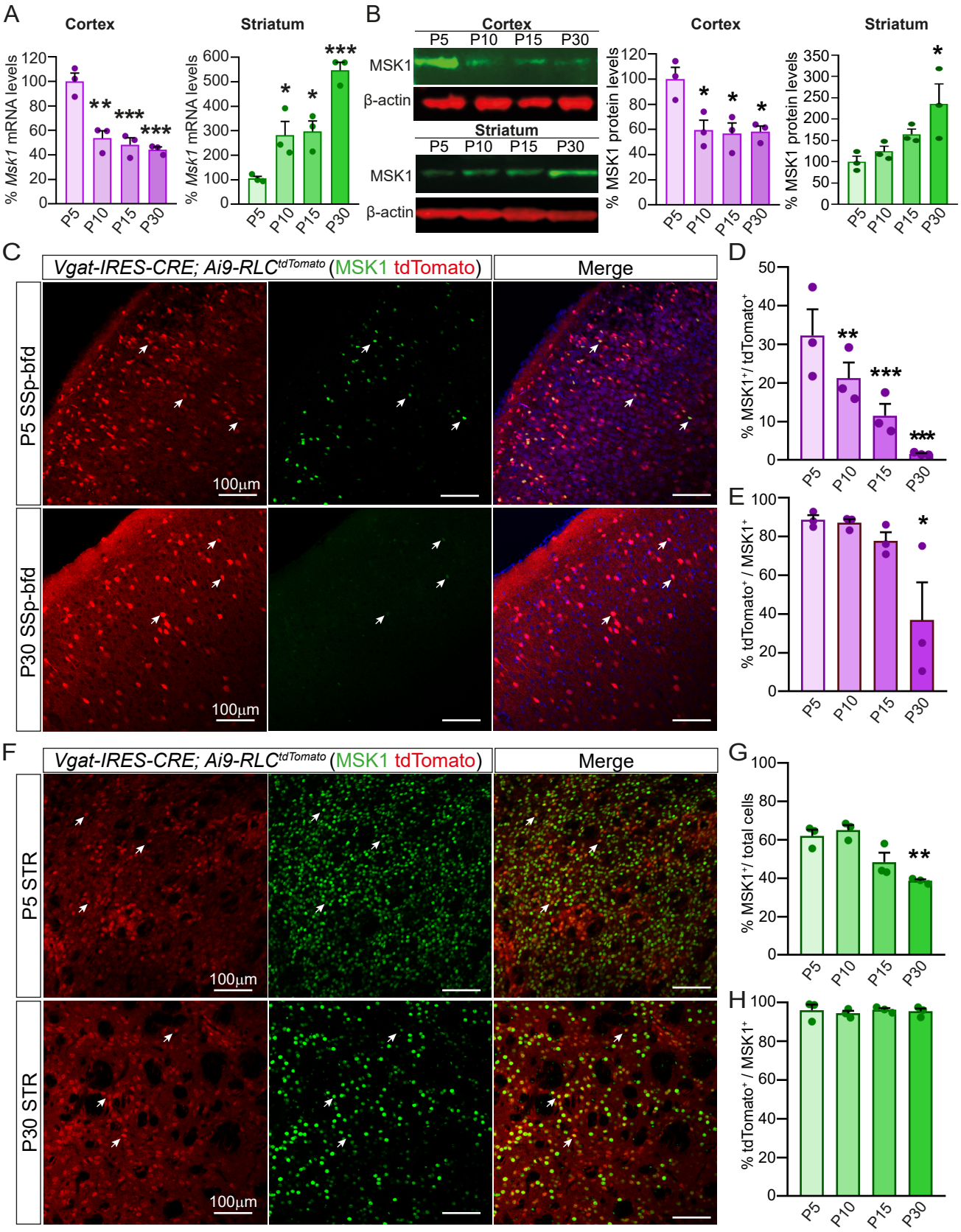
A
Cortex
Striatum
% Msk1 mRNA levels
P5
P10
P15
P30
B
Cortex
Striatum
MSK1
β-actin
% MSK1 protein levels
C
Vgat-IRES-CRE; Ai9-RLCtdTomato (MSK1 tdTomato)
Merge
P5 SSp-bfd
P30 SSp-bfd
100µm
D
% MSK1+/ tdTomato+
E
% tdTomato+ / MSK1+
F
P5 STR
P30 STR
G
% MSK1+/ total cells
H
% tdTomato+ / MSK1+

Figure 1

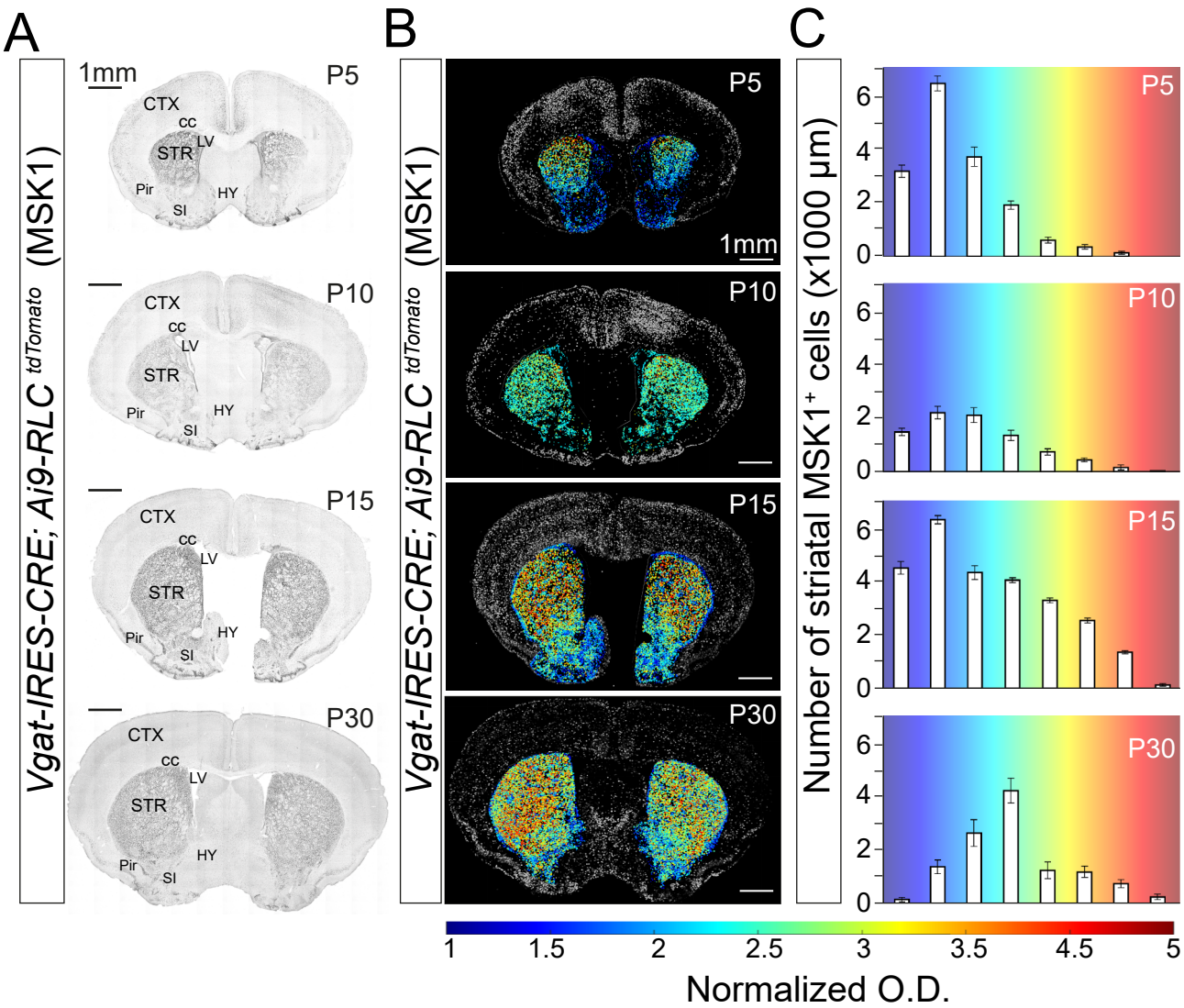
A
B
C
Vgat-IRES-CRE; Ai9-RLC tdTomato (MSK1)
1mm
P5
P10
P15
P30
CTX
cc
LV
STR
Pir
HY
SI
Number of striatal MSK1+ cells (x1000 µm)
0
2
4
6
1
1.5
2
2.5
3
3.5
4.5
5
Normalized O.D.

Figure 2

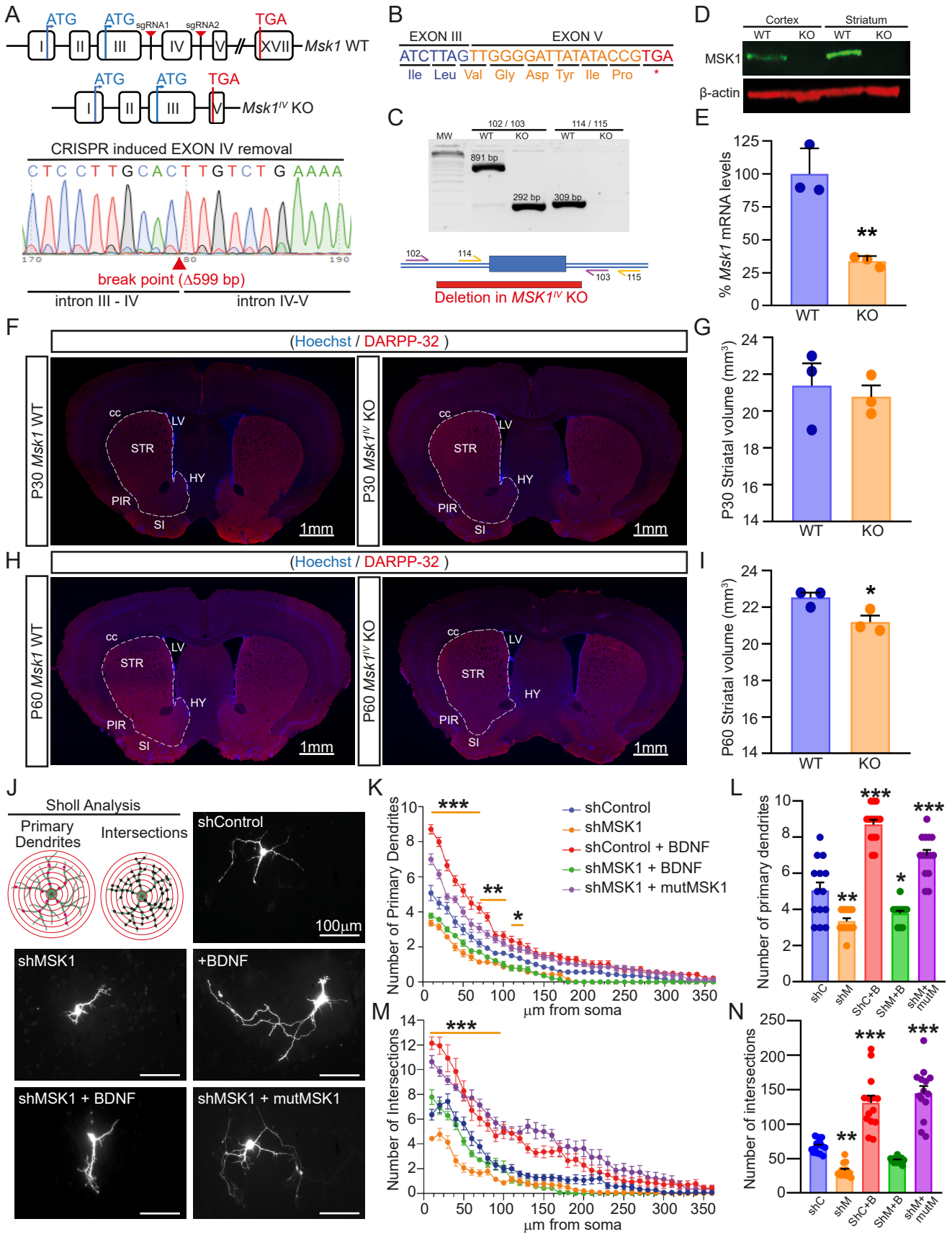
A
ATG
ATG
sgRNA1
sgRNA2
TGA
I
II
III
IV
V
XVII
Msk1 WT
ATG
ATG
TGA
Msk1IV KO
CRISPR induced EXON IV removal
CTC CTTGCACTTGTCT G AAAA
break point (Δ599 bp)
intron III - IV
intron IV-V
B
EXON III
EXON V
ATCTTAGTTGGGGATTATATACCGTGA
Ile Leu Val Gly Asp Tyr Ile Pro *
C
MW
102 / 103
114 / 115
WT KO WT KO
891 bp
292 bp
309 bp
102
114
103
115
Deletion in MSK1IV KO
D
Cortex
Striatum
WT KO WT KO
MSK1
β-actin
E
% Msk1 mRNA levels
125
100
75
50
25
0
**
WT
KO
F
(Hoechst / DARPP-32)
P30 Msk1 WT
P30 Msk1IV KO
cc
LV
STR
HY
PIR
SI
1mm
G
P30 Striatal volume (mm3)
24
22
20
18
16
14
WT
KO
H
(Hoechst / DARPP-32)
P60 Msk1 WT
P60 Msk1IV KO
cc
LV
STR
HY
PIR
SI
1mm
I
P60 Striatal volume (mm3)
24
22
20
18
16
14
*
WT
KO
J
Sholl Analysis
Primary Dendrites
Intersections
shControl
100µm
shMSK1
+BDNF
shMSK1 + BDNF
shMSK1 + mutMSK1
K
Number of Primary Dendrites
shControl
shMSK1
shControl + BDNF
shMSK1 + BDNF
shMSK1 + mutMSK1
***
**
*
µm from soma
L
Number of primary dendrites
***
**
*
***
shC
shM
ShC+B
ShM+B
shM+ mutM
M
Number of Intersections
***
µm from soma
N
Number of intersections
***
**
***
shC
shM
ShC+B
ShM+B
shM+ mutM

Figure 3

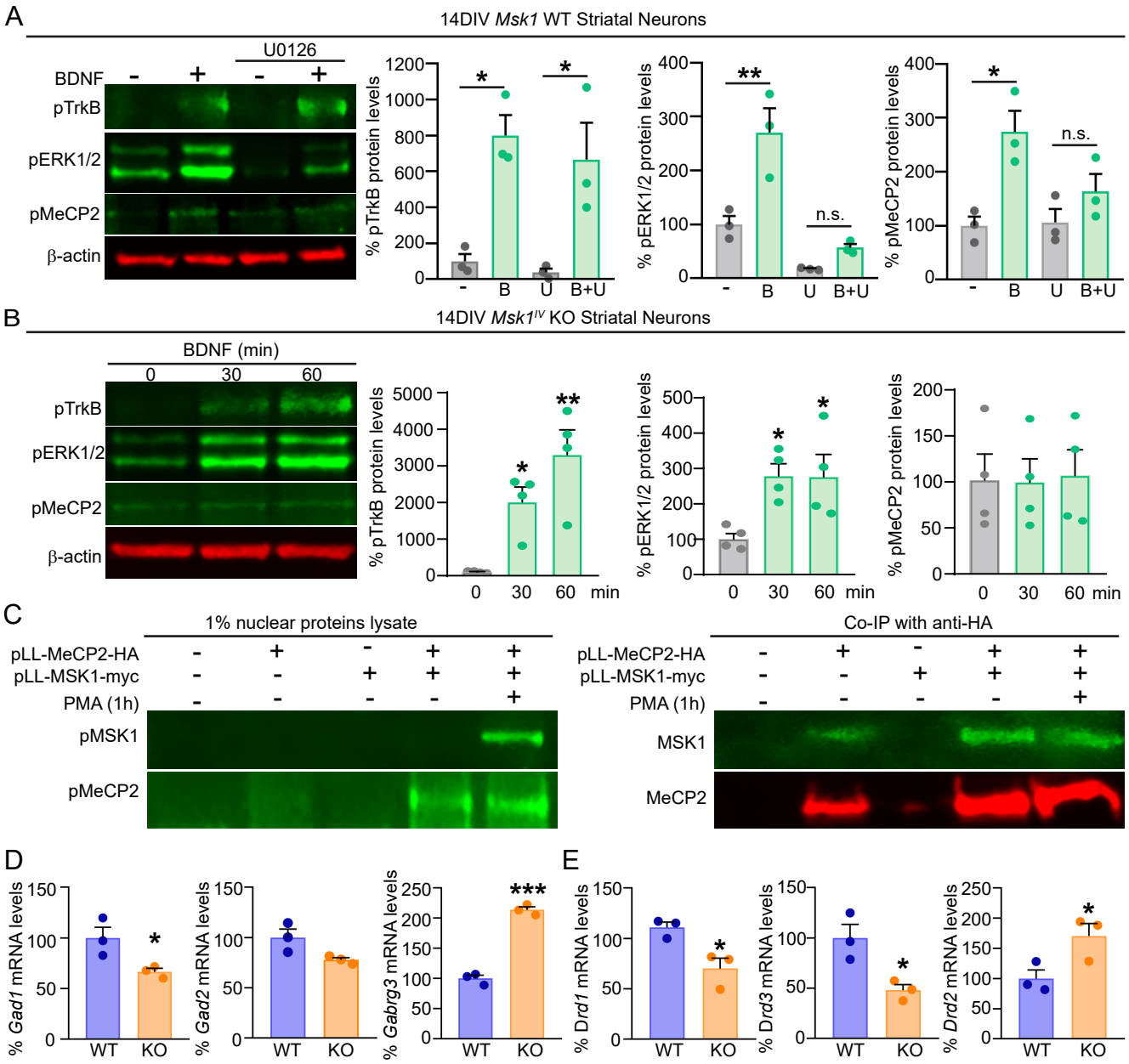
A
14DIV Msk1 WT Striatal Neurons
U0126
BDNF - + - +
pTrkB
pERK1/2
pMeCP2
β-actin
% pTrkB protein levels
% pERK1/2 protein levels
% pMeCP2 protein levels
- B U B+U
n.s.
B
14DIV Msk1IV KO Striatal Neurons
BDNF (min)
0 30 60
min
C
1% nuclear proteins lysate
Co-IP with anti-HA
pLL-MeCP2-HA
pLL-MSK1-myc
PMA (1h)
pMSK1
pMeCP2
MSK1
MeCP2
D
E
% Gad1 mRNA levels
% Gad2 mRNA levels
% Gabrg3 mRNA levels
% Drd1 mRNA levels
% Drd3 mRNA levels
% Drd2 mRNA levels
WT KO

Figure 4

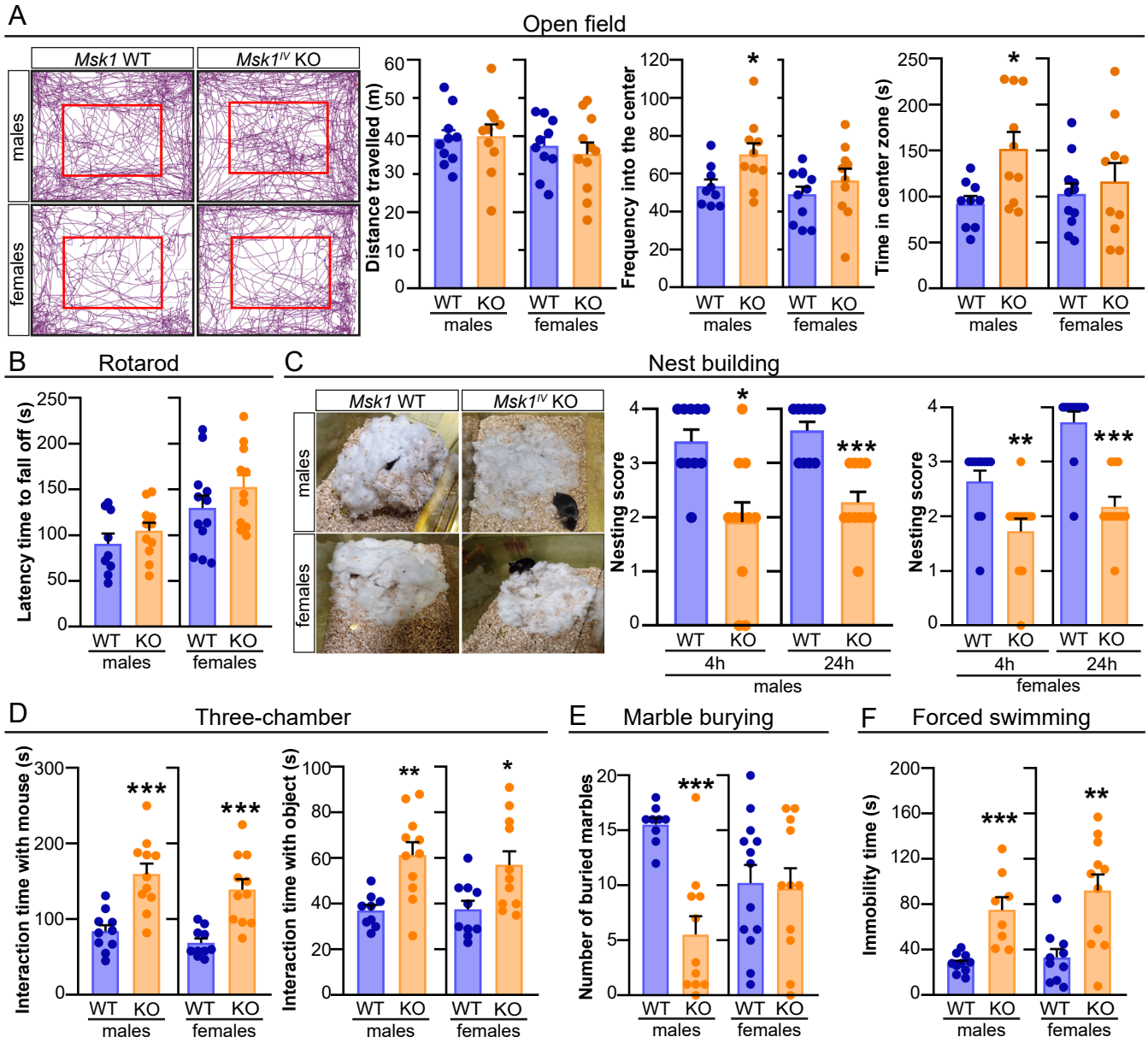
A
Open field
Msk1 WT
Msk1IV KO
males
females
Distance travelled (m)
Frequency into the center
Time in center zone (s)
WT KO
males
females
B
Rotarod
Latency time to fall off (s)
C
Nest building
Nesting score
4h
24h
D
Three-chamber
Interaction time with mouse (s)
Interaction time with object (s)
E
Marble burying
Number of buried marbles
F
Forced swimming
Immobility time (s)

Figure 5

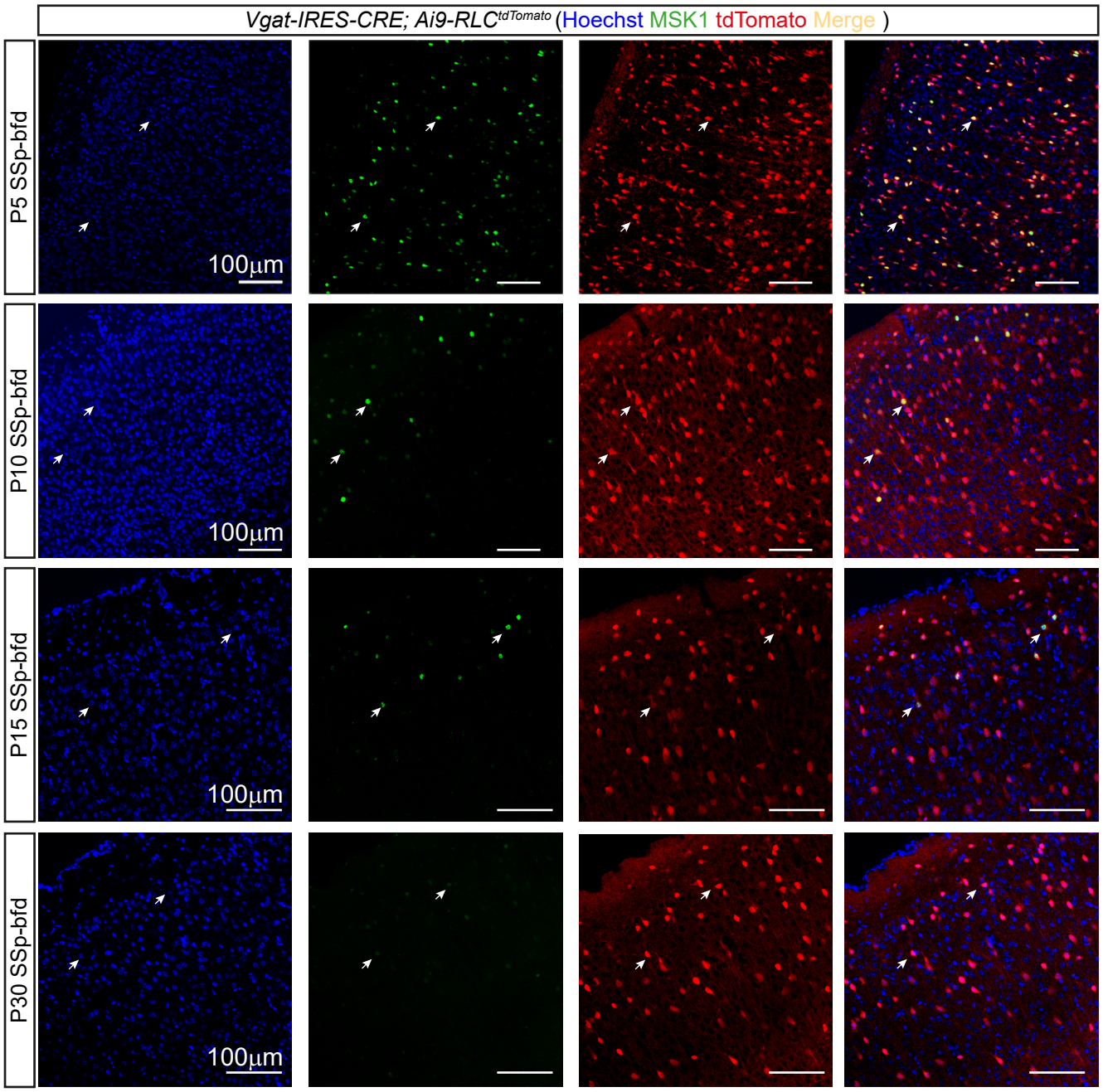

Supplementary Figure 1

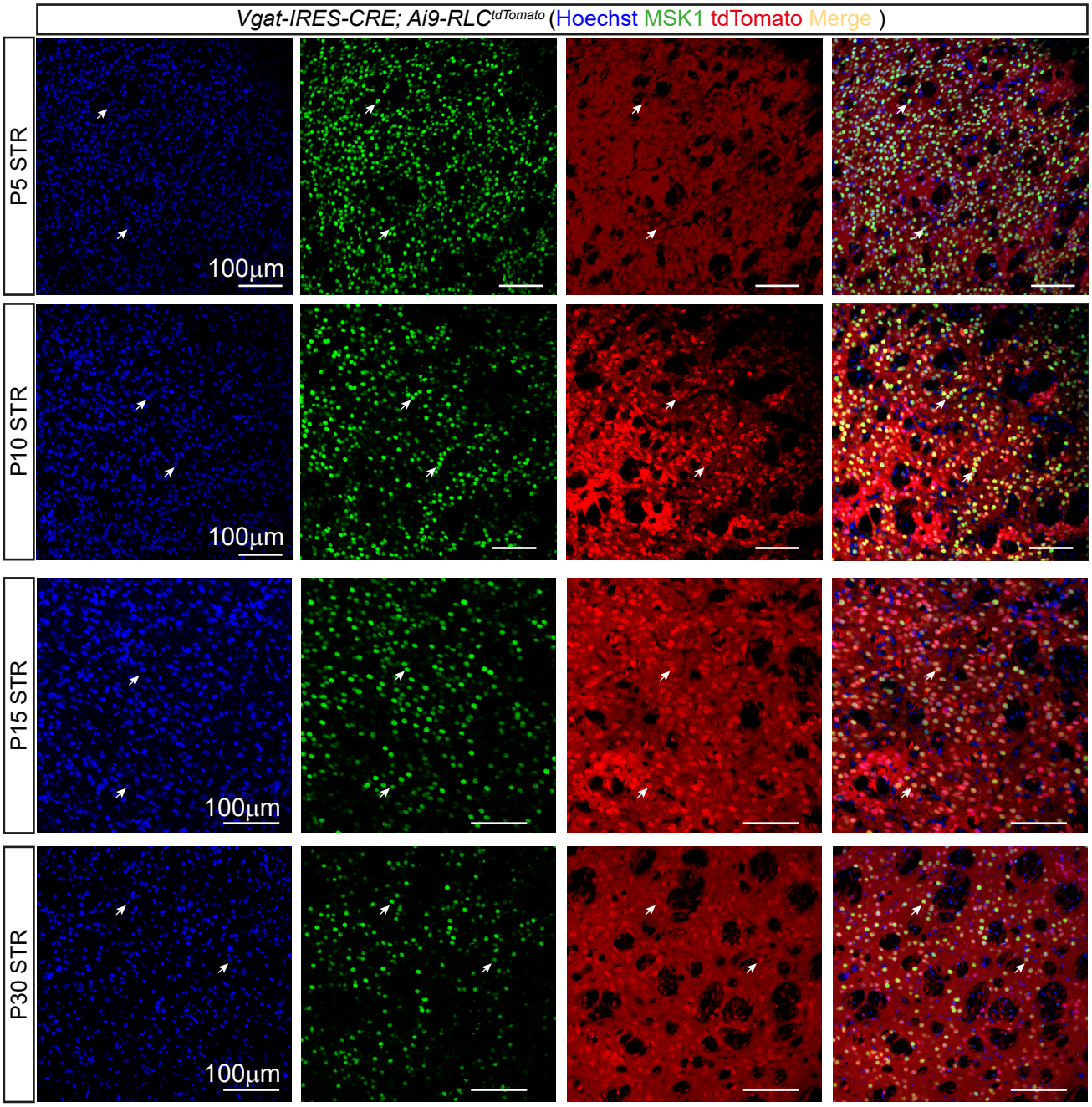

Supplementary Figure 2

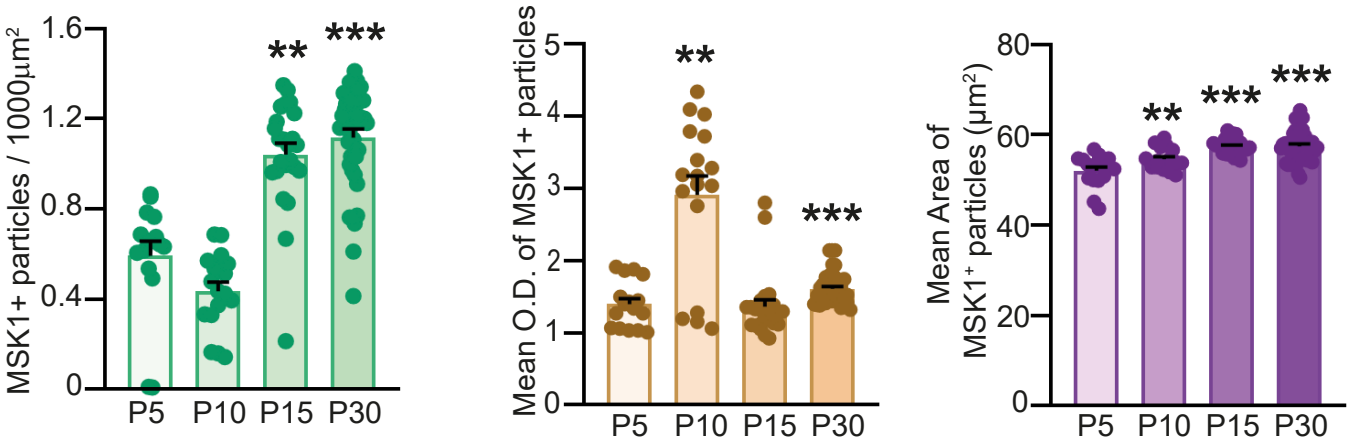

Supplementary Figure 3

Supplementary Figure 4

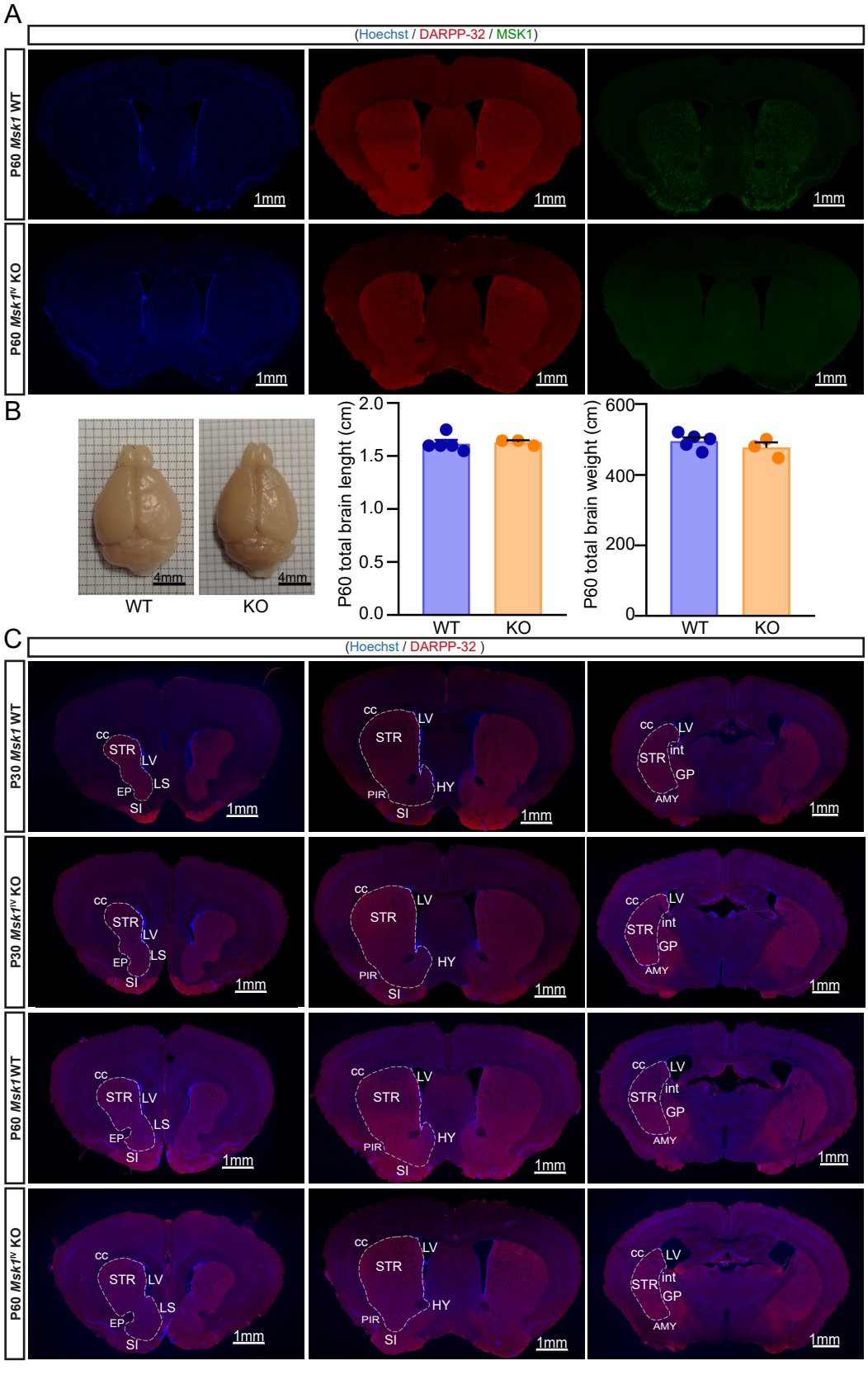

A

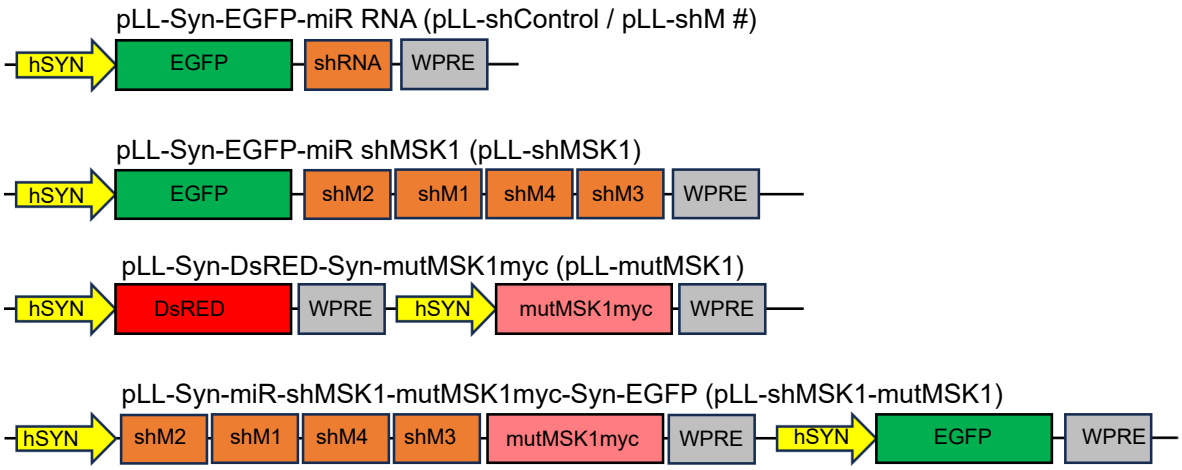

B

miR-based shM1: AGAATATGCTCTTTCAGTTTC

wt MSK1: GAAACTGAAAGAGCATATTCT
mut1 MSK1: GAGACCGAGAGAGCATATTCT
Glu Thr Glu Arg Ala Tyr Ser

miR-based shM2: TGAAGAGGATCTATGACAGCT

wt MSK1: AGCTGTCATAGATCCTCTTCA
mut2 MSK1: AGCCGTCATCGACCCTCTTCA
Ala Val Ile Asp Pro Leu

miR-based shM3: TACATTAGAACACCTAAGCTC

wt MSK1: GAGCTTAGGTGTTCTAATGTA
mut3 MSK1: GAGCCTGGGTGTCCTAATGTA
Ser Leu Gly Val Leu Met

miR-based shM4: AAAGGTTGCTTTCACACAGGT

wt MSK1: ACCTGTGTGAAAGCAACCTTT
mut4 MSK1: ACCTGCGTGAAGGCGACCTTT
Thr Cys Val Lys Ala Thr Phe

C

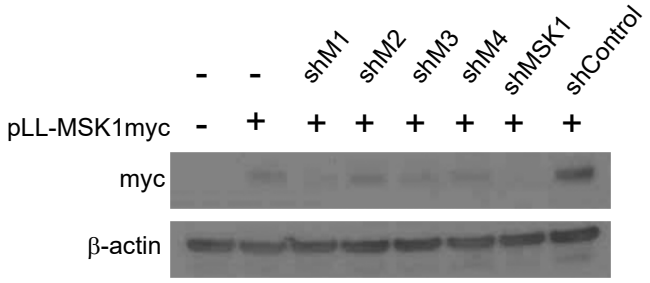

Supplementary Figure 5

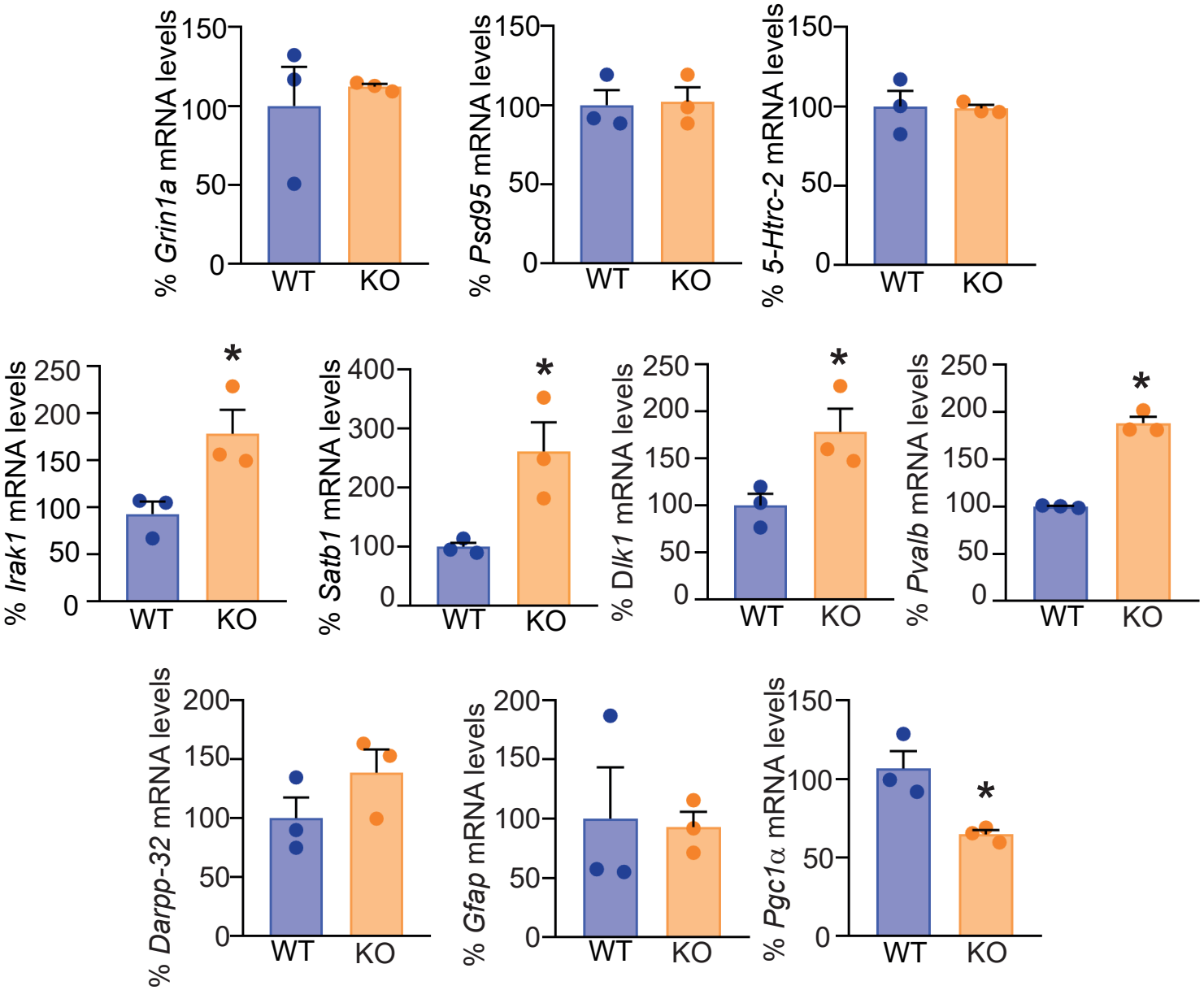

Supplementary Figure 6

Supplementary Information

Animals.

All of the experiments using mice were conducted with permission from the Council of Agriculture and Livestock of Castille and Leon Government, after approval by the ethical committee of the University of Salamanca and following the European Directive 2010/63/EU and the Spanish Royal Decree 53/2013-Law 32/2007. All animals were kept on a 12:12 light/dark cycle, receiving food and water *ad libitum*. *Vgat-CRE; Ai9* mice were generated by breeding the mouse lines Vgat-IRES-CRE (B6J.129S6(FVB)-*Slc32a1*$^{tm2(cre)Lowl/MwarJ}$; JAX stock #028862; Vong et al., 2011) with mice Ai9 (B6.Cg-*Gt(ROSA)*$^{26Sortm9(CAG-tdTomato)Hze/J}$; JAX stock #007914; Madisen L et al., 2010). Founder (F_0) *Msk1*^{IV} KO mouse was bred with C57BL/6 mice obtained by local breeding, and heterozygous offspring were back-crossed to C57BL/6J mice for 4 generations before establishing the mouse line *Msk1*^{IV} KO (B6-Rps6ka5^{em3SAL}).

Quantitative Real-Time PCR (qPCR).

cDNA was synthesized using the ReverAid retrotranscriptase (ThermoFisher; Manufacturer instructions) from 0.5μg of total RNA isolated from cortex or striatum using Trizol (Invitrogen; Manufacturer instructions). qPCR was performed using Sybr™ Green PowerUp™ mix (Applied Biosystems™; Manufacturer instruction) and specific primers for *Msk1, Gad1, Gad2, Gabrd, Drd1, Drd2, Drd3, Grin1a, Psd95, 5-Htrc-2, Irak1, Satb1, Dlk1, Pvalb, Darpp-32, Gfap, Pgc1α* and *Tbp* (see table 1) on a QuantStudio™ 7 Real-Time PCR System (ThermoFisher). Data were analysed using the $2^{-\Delta\Delta Ct}$ method.

Quantitative Western Blot.

Total protein lysates were obtained in RIPA buffer (Tris-HCl 25mM pH7.5, NaCl 150mM, TritonX-100 1%, sodium deoxycholate 1%, and SDS 0.1%) containing protease and phosphatase inhibitors (Pierce, Thermofisher) and quantified by the BCA method (Pierce Protein Assay,

Thermofisher; Manufacturer instructions). Equal amounts of total protein (25-35μg) were loaded and separated by electrophoresis in Bis-Tris 10% acrylamide gels. After, proteins were transferred to Immobilon-FL PVDF membranes (Merck-Millipore) and washed twice in TBS buffer followed by incubation in Intercept-TBS Blocking Buffer (Li-COR; Manufacturer instructions). Antibodies and concentrations were as follow: rabbit monoclonal anti-MSK1 (C27B2; Cell Signaling) 1:1000, mouse monoclonal anti-β-actin (669-1-Ig; Proteintech) 1:20000, mouse monoclonal anti-phospho-pan-Trk (#9141; Cell Signaling) 1:1000, rabbit polyclonal anti-MeCP2 phospho S421 (ab254050; Abcam) 1:500, mouse monoclonal anti-pERK1/2 (#9101; Cell Signaling) 1:3000, mouse monoclonal anti-Myc (sc-41; SantaCruz) 1:200, mouse monoclonal anti-MeCP2 (Quimigen 10861-1-AP) 1:500; rabbit polyclonal anti-MSK1 phosho Thr581 (#9595; Cell Signaling). Fluorescent secondary antibodies used were: IRDye 800CW Donkey anti-rabbit IgG (926-32213; Li-COR) 1:20000 and IRDye 680LT Donkey anti-mouse IgG (926-68022; Li-COR) 1:20000. Images were capture using a Li-Cor Oddysey XF system. Fluorescent images were acquired using an Odyssey XF Imaging system (Li-Cor) and densitometry analyzed by Empiria Studio™ Software.

Immunohistochemistry.

Mice were deeply anesthetized with sodium pentobarbital (60mg/kg body weight; i.p.), and perfused transcardially, first with ice-cold PBS 1X (70mL) followed by the same volume of ice-cold PFA 4% in PBS. Brains were extracted and post-fixed for 3h in PFA 4% at 4ºC before immersion in sucrose 30% at 4ºC for 48h. Afterwards, 40µm-thick coronal brain sections were obtained using a cryotome (Thermo Scientific ™, Microm™ HM 430). For colocalization, densitometric, and volumetric assays every 10th section was used. Brain slices were collected in antifreeze solution (Glycerol 30%, Ethylene Glycol 30%, in PBS) and stored at -20ºC until use.

For immunofluorescent assays, brain slices were rinsed twice in PBS 1X followed by a 10 min permeabilization step with Triton X-100 0.25% in PBS, and a 2h blocking step in a solution containing Triton X-100 0.3%, normal donkey serum 10% (0.17-000-121: Jackson ImmunoResearch) and bovine serum albumin 5% (BSA, MB04602; NZYtech) in PBS. After, slides were incubated for 24 hours at 4ºC with MSK1 and DARPP-32 antibodies diluted in antibody solution (Triton X-100 0.3%, normal donkey serum 5% and BSA 1% in PBS). After, the slices were washed 4 times in PBS 1X at RT for 15 min, followed by 1h incubation in the dark with antibody solution containing the secondary antibodies and 4μM Hoechst 33258. After 3x 10 min washes in PBS, tissue slices were mounted onto Superfrost glass-slides previously coated with gelatine solution (Tris-HCl 50mM pH7.5, gelatine from porcine skin 0.2 %) and let dry at RT protected from light. The sections were after glass covered using a Mowiol/DABCO mounting solution (Mowiol 4-88 0.1%, glycerol 0.26%, DABCO 2.5%, Tris-HCl 0.1M pH8.5). Finally, the slides were kept protected from light at 4ºC until visualization.

For densitometry assays, brain slices were rinsed twice in Phosphate Buffer (PB) 0.1M followed by a 10 min incubation with H_2O_2 and Methanol (1 part of Methanol, 1 part of H_20_2 30% and 8 parts of PB 0.1M). Later, the slices were washed 3 times in PB 0,1M for 5 min each at RT, followed by other 2x 5 min washes in TBS-T solution (Triton X-100 0.3% in TBS). Then, the slices were incubated for 24-48 hours at 4ºC with antibody solution containing MSK1 antibody. After, the slices were rinse twice in TBS-T solution and incubated for 2h at RT with anti-mouse biotinylated secondary antibodies (BA-2000; Vector) diluted 1:200 in antibody solution. Sections were washed 2x 5 min in TBS-T and incubated for 3h at RT in avidin/biotin-peroxidase solution (PK-4000, Vectastain), followed by 2x 5 min washes with Tris-HCl 0.05M before been placed for 25 min in developing solution (3,3-diaminobenzidine tetrahydrochloride, DAB; Sigma-Aldrich, D-9015)

with 0.006% H_2O_2. Slides were washed twice with a Tris-HCl 0.05 M solution and mounted onto Superfrost glass slides previously coated with 0,2% gelatine and let dry overnight. Finally, sections were dehydrated 3x in ethanol 100% for 1 min and 2x in xylol for 3 min, glass covered using Entellan™ and kept at RT until visualization.
The following primary antibodies were used: rabbit monoclonal anti-MSK1 (C27B2; Cell Signaling) 1:1500, rabbit monoclonal anti-DARPP-32 (271111, Santa Cruz) 1:500. The secondary fluorescent antibodies used were donkey-anti-rabbit-Alexa 488 (21206; ThermoFisher) 1:400, donkey-anti-mouse-Alexa-555 (31750; ThermoFisher) 1:400.

Densitometry quantification.

High-resolution microphotographs (digital resolution of 132pixel/100μm^2) were taken at 10X magnification under a Leica DMRX microscope with an MBF camera (MBF Bioscience CX9000; Williston, VT, USA) to prepare whole-section digital mosaics using the Neurolucida software (NL-Vs 8.0, MicroBrightField®, Inc., Williston, VT, USA). To set homogeneous microscopic illumination conditions and to calibrate optical density (OD) measurements, photographs were taken using a standardized grayscale range and a stepped density filter (11 levels) (®EO Edmund industrial optics-ref 32599, Karlsruhe, Germany). For morphometrical analysis, immunoreactive neurons were segmented by density thresholding using ImageJ software and the Maximum Entropy algorithm. Coordinates, area, and O.D. values of the segmented cells were collected to perform statistical analysis and to build MSK1 expression maps (MATLAB). O.D. was used as measurement of the intensity of the immunoreactivity of each cell. Normalized O.D. values of immunoreactive cells were calculated by subtracting the mean O.D. of the whole section from the O.D. values of segmented particles, divided by the gray standard deviation of the whole slice. The number of segmented cells was normalized to N/10,000μm^2 of surface area. Extensive full-sections maps encoding

the location, area and density of segmented particles were made using MATLAB software (MATLAB R-2017, Scatterplot function). O.D. was converted into color with the MATLAB color scale Jet from the Scatterplot function.

Msk1^{IV} KO mouse line generation.

The *Msk1^{IV}* KO mouse line was generated by CRISPR/Cas9 edition in a C57BL/6J background. We designed specific crRNAs using the *Breaking Cas* application from the Spanish National centre of Biotechnology (https://bioinfogp.cnb.csic.es/tools/breakingcas/). Two specific crRNAs (Table 2) flanking *Msk1* Exon IV were selected for its removal. Previous to the microinjection, 5μL of each crRNA (250ng/μL) and 10μL of tracrRNA (250ng/μL) were annealed together to form the sgRNAs. To form the ribonucleoprotein complexes, 1μL of each sgRNAs was thereafter mixed with 1.2μL (300ng/μL) of *S. pyogenes* Cas9 (Integrated DNA Technologies) in 9.2μL of microinjection buffer (Integrated DNA Technologies) and incubated for 15min at RT. The Cas9/sgRNAs complexes were microinjected using borosilicate needles into the biggest pronucleus of one-cell C57BL/6J mouse zygotes at the Transgenic Facility (NUCLEUS, platform for research support of the USAL/IBSAL). The injected zygotes were kept at 37ºC and 5% CO_2 in KSOM media until the next day, when 15 to 20 viable 2-cell embryos were implanted into pseudo-pregnant CD-1 female mice. The offspring was characterized by PCR (Supplementary Table 3; MSK1 Forward and MSK1 Reverse primers) and the promising PCR products were analysed by Sanger sequencing in order to determine the modification generated by the system. Founder animals (F_0) were back-crossed to C57BL/6J wild-type mice to generate F1 *Msk1$^{IV/+}$* mice. To detect the absence or presence of the mutant allele we used the primers 102/103 and 114/115 (Supplementary Table 3).

Striatal volumetric analysis.

Each brain was totally coronal sectioned using a cryotome (40μm thickness) and divided in 10 consecutive series. After identifying the correct series containing the first coronal cut of the striatum (Bregma +1.845mm; Allen Brain Reference Atlas) we did immunostaining assays as previously described using anti-DARPP-32 antibodies. Nuclei were counterstained with Hoechst 33258. Single plane tile scan confocal images were acquired at a 1024x1024 pixel resolution on an inverted Leica Stellaris 8 confocal microscope. 9 to 12 sections covering the striatum along the rostrocaudal axis were imaged using the same laser powers, gain, and detection filters. Both hemi-striata from each acquire image were delineated using the Allen Brain Reference Atlas as a guide and the area calculated using the ImageJ-Fiji software. To estimate the total volume, we applied the mathematical formula of Cavalieri´s principle $Vc = d \sum_{i=1}^{n}(A_i)$, considering the distance between each brain slice (d), the calculated area of the striatum from each coronal section (A_i) and the number of sections which contain the striatum (n).

Primary striatal cultures.

Striatal cultures were prepared from E14.5 – E.16.5 mouse striata dissected in PBS-GB (D-Glucose 0.5%, BSA 0.1 %, Penicillin 10μg/mL, Streptomycin 10μg/mL). Tissue was dissociated by incubation with Trypsin-EDTA (0.25 %) solution (25200056; Gibco) at 37ºC for 30min, gently inverting the tube 3 to 4 times every 5 min, followed by mechanical disaggregation with a 10mL plastic pipette. Dissociated tissue was then diluted 1:1 with trypsin neutralizer solution (Neurobasal medium (Gibco), glutamine 0.2 mM (Gibco), NCS21 2% (Capricorn Scientific), trypsin inhibitor 0.035% (STEMCELL), DNase I (Sigma-Aldrich), resuspended with a 10mL pipette, filtered through a 40μm cell strained (BD) and centrifuge for 5min at 800g and RT. Cell pellet was thereafter resuspended in supplemented Neurobasal media (NCS21 2%, Penicillin 10 μg/mL, 10 μg/mL, glutamine 0.2 mM, HEPES

10 mM) and cells were plated at a density of $0.3x10^5$ cells/cm^2 onto cell culture vessels or glass coverslips treated overnight with a solution containing Poly-D-Lysine hydrobromide (100μg/mL; 70000-150000 MW; Sigma-Aldrich) and Laminin (10μg/mL; CF858, Corning).

HEK293-FT cell cultures.

Cells were grown in supplemented DMEM (21699035; Gibco) (FCS 10%, glutamine 2mM, HEPES 10mM, Penicillin 10μg/mL, Streptomycin 10μg/mL, MEM non-essential amino acids 1X, 2-mercaptoethanol 0.001%). Cells were maintained at 37ºC, 5 % CO_2 and 95% humidity. Cultures were tested regularly for mycoplasma (6601; TaKaRa PCR Mycoplasma Detection Set).

Plasmid generation.

All vectors are based on the previously described dual-promoter lentiviral vector pLL-hSYN-DsRED-hSYN-EGFP (83), which basically contains two human Synapsin promoters able to transcribe efficiently and independent from each other the cDNAs located downstream of them. The Synapsin promoter is highly specific for neurons in primary cultures of cortical neurons.

Generation of shRNA expression vectors: The shRNA expressing vectors were generated as previously described (84). The specific miRNA-based shRNA against the mouse open reading frame (ORF) for MSK1 were generated using the BLOCK-iT™ RNAi Designer software (Invitrogen) and cloned into the pcDNA6.2-GW/miR vector according to instructions provided by the manufacturer. Positive clones were sequenced by PCR, and the miRNA-based shRNA cassettes, resulting from digestion with the restriction enzymes BamHI and NotI, were cloned into the pLL-hSYN-DsRED-hSYN-EGFP vector (Gascon et al., 2008) or clone together into the pcDNA6.2-GW/miR vector into the BglII and NotI following manufacturer instructions. Positive clones including the 4 miRNA-based shRNAs were confirmed by Sanger sequencing before been clone into the pLL-hSYN-DsRED-hSYN-EGFP

vector to generate the pLL-shMSK1 vector. The oligonucleotides used to generate the miRNA-based shRNAs are listed in Supplementary Table 4.

Generation of MSK1 expression vectors: The open reading frame for MSK1 was amplified by PCR from cDNA obtained from C57BL/6J WT mouse brain using the primers MSK1 BamHI-Forward, MSK1 NotI-Reverse, MSK1 NotI-myc-Reverse (Supplementary Table 5) The PCR product was purified using an agarose gel and co-digested with BamHI and NotI restriction enzymes (New England Biolab) and directly cloned into the pLL-hSYN-hSYN-GFP vector at the BamHI and NotI restriction sites located downstream of the first hSYN promoter. Transformed bacterial colonies were screened by PCR and positive clones were subsequently verified by analysis using restriction enzymes. The MSK1 and MSK1-myc sequences were confirmed by PCR sequencing using specific primers for mouse MSK1 (MSK1-440, MSK1-532, MSK1-955, MSK1-1490, MSK1-1964; Supplementary Table 5). The MSK1-myc plasmid was mutated to made it resistant to the miRNAs-based shRNAs using the oligonucleotides mut-shM1, mut-shM2, mut-shM3, mut-shM4 (Supplementary Table 5) and the QuikChange Multi Site-Directed Mutagenesis kit (200514; Agilent; Manufacturer Instructions) in several assays until all the mutations were incorporated. All the PCR products were analysed by Sanger sequencing (primers MSK1-440, MSK1-532, MSK1-955, MSK1-1490, MSK1-1964) . The final product was then PCR amplified with the oligos BamH1-Forwad and NotI-myc-Reverse (Supplementary table 5) to clone into the pLL-shMSK1 digested with the same restriction enzymes in order to generate the pLL-shMSK1-mutMSK1 vector. The final vector pLL-mutMSK1, containing the coding sequence for the reporter protein DsRED, was generated by amplification of the mutMSK1-myc sequence with the oligos MSK1 NheI Forward and the MSK1 EcoRI-myc-Reverse

(supplementary table 5). The pLL-MeCP2-HA expression vector was generated as previously described (Yazdani, Deogracias et al., 2012).

Cell transfection.

Striatal neurons cultured on 24 well plates containing 14 mm diameter coverslips treated with poly-D-lysine and laminin, were transfected 2 days after plating with 1μg of total DNA with FuGENE 6 transfection reagent (E2691; Promega) at a ratio 1:3.

HEK293-FT cells were plated the day before transfection at a density of 75000 cells per cm^2. Medium was replaced by fresh DMEM supplemented as before 1h before transfection. For transfection, plasmids were diluted in DMEM and incubated for 20min at RT with Polyethylenimine (PEI, 23966, Polysciences) at a ratio 1:3 DNA:PEI. 24h after transfection medium was replaced and cells were maintained for 48h after transfection before been collected for obtain total protein lysates or nuclear lysates.

Immunocytochemistry and neuronal morphology analysis.

Striatal neurons were fixed by adding directly to the medium an equal amount of a PBS solution pH7.4 containing PFA 8% and sucrose 8%. Cells were kept for 20min at RT and then washed three time with PBS. Blocking solution was applied for 1h (0.1% Triton X-100, 10% normal donkey serum, 5% BSA), and primary antibodies against EGFP (MA1-952; ThermoFisher) diluted 1:200 in antibody solution (0.1% Triton X-100, 10% normal donkey serum, 1% BSA) were applied for 24h at 4ºC without shaking. After 3 washes with PBS, donkey-anti-rabbit-Alexa 488 (21206; ThermoFisher) diluted 1:400 in antibody solution containing Hoechst 33258 were applied and kept in the dark at RT for 1h, washed 2 times in PBS and mounted onto glass slides using Mowiol/DABCO mounting media.

Transfected neurons expressing EGFP were visualized using standard epifluorescence under a 5x Neofluar objective. Scholl analyses were performed manually with the help of the NIG ImageJ software, setting

the origin of the concentric circles in the centre of the soma and separated each 10μm. A maximum length of 350 μm from the soma was analysed in order to determine the length of the neuronal arborization.

Purification of nuclear protein lysates.

Cells were collected on ice-cold-PBS, centrifuge at 800g for 5min at 4ºC and resuspended in 10 vol. of 250-STM buffer (sucrose 250mM, Tris-HCl 50mM pH8.0, MgCl2 5mM, NP-40 0.5%, proteases and phosphatases inhibitors). After 10min incubation on ice, cells were centrifuged at 800g for 10min at 4ºC. The pellet was resuspended in 1 vol. of Nuclear Lysis Buffer (Tris-HCl 20mM pH7.5; KCl 300mM, EDTA 0.2mM pH8.0, NP-40 0.1%, glycerol 20% and proteases and phosphatases inhibitors) and incubated for 30min on ice before been centrifugated at 12000g for 30min at 4ºC. The supernatant, containing the nuclear proteins, was aliquoted and stored at -20ºC.

Co-immunoprecipitation assays.

To determine the interaction between MSK1 and MeCP2 independently of the cell context, co-immunoprecipitation was carried using magnetic beads coupled to anti-HA antibodies (SAE0197, Sigma-Aldrich; Manufacturer instructions) on nuclear protein lysates from HEK293-FT cells co-transfected with expression plasmids for MSK1-myc and MeCP2-HA. Immunoprecipitated proteins were thereafter analysed by western blot using monoclonal anti-MSK1 antibody (#3489; Cell Signaling) 1:1000 and polyclonal antibodies anti-MeCP2 (10861-1-AP; Quimigen) 1:500 as control of the immunoprecipitation step.

Behavioural tests.

All the behavioural tests were performed at the Institute of Neurosciences of Castille and Leon (INCyL) animal facility, between 12:00pm and 15:00pm, considering a room with stable temperature, humidity, light intensity and avoided from noises. Before each test, mice were acclimated during 30min in individual homecages.

Open field test: Anxiety-like behaviors, exploration and movement were evaluated using this test. Open field arena was made of white fully opaque plexiglas. Square base is 50cm x 40cm and walls are 30 cm high to avoide mice to jump over. Mice were placed in the center of the arena and let to free explore during 10 minutes. Measurements as distance travelled (cm), time spent (sec), and number of entries in center or periphery zones were taken and analyzed with tracking software (ANY-maze).

Rotarod: Tasks were run with a Rotarod LE 8300 (LSI Letica) to measure motor coordination and balance. Mice were trained for 2 consecutive days before test. Rotarod conditions were setup to increase from 4 rpm to 40 rpm in 5min. Each task was repeated three times, with a 10 min interval between each repetition. Measurements taken were time till fall or time spent on the apparatus (sec) and velocity reached (rpm).

Three Chamber Social Test: This task evaluates social approach and interaction with novel inputs. Arena was made of white fully opaque plexiglas and consists of three spaces: middle chamber (where mice are placed to start the test, empty), left chamber (where new and same gender conespecific mouse was situated inside of a cage) and right chamber (where a new object, an orange Lego piece, is placed inside a cage). Mice were allowed to see and sniff freely in the three chambers. In this case, we do not focus on novelty analysis, because both stimuli are new. Our main interest was to assess interaction and exploration differences between conespecific mouse and objects. Habituation was made by placing the mice into the arena with all of the three chambers empty, being them capable of moving freely. Tests start with mouse placed in the empty middle chamber, from where mouse explores and moves between chambers during 10 minutes. Interaction time was measured as the time (sec) the mice spent

sniffing around the cages. Trials were recorded and further analyzed using the tracking software *ANY-maze*.

Marble Burying Test: This test assesses explorative behaviors and anxiety-like symptoms. Arena consists of homecages filled with 5 cm thick sawdust, with 20 marbles placed on top of it, displayed in 4 rows of 5 marbles each. Each mouse had 30 minutes to freely move and interact with the marbles. We count the number of buryed marbles , considering a marble as buryed if it had 2/3^{rds} covered by the sawdust.

Nesting Test: This test evaluates mice capacity to build a place to sleep, hibernate or reproduct. Mice are given a cotton piece (5.1 – 5.2 g) placed in the upper left corner of a homecage filled with 0.5 cm sawdust. Using the parameters described by Lewarch and Hoekstra (2018), score was assigned to the cotton/nest status at 4h and at 24h of starting the test.

Forced Swimming Test: Mice were individually forced to swim in a 5L Beaker glass (FB33119, 270mm height, 170mm internal diameter) filled with 2.5L of fresh water (25°C ± 1°C) for 7min. The water was replaced after each trial. Tests were filmed to further analysis of freezing time (sec), a measure of depression-like mice behaviour.The first 2 minutes were not considered to avoid effects caused by the mice stablishment in the Beaker glass.

Statistical analysis.

All statistical analysis were performed using GraphPad Prism 8.0, except the statistical analysis of the densitometry assays that were performed using the IBM SPSS software, version 26. All error bars shown on graphs represent ± standard error of the mean. The statistical tests used in are indicated in the figure legends. Group differences in the number of immunoreactive cells, area and OD were determined using the non-parametric Kruskal-Wallis test.

Supplementary Table 1: Primers used for qPCR assays.

GENE	Forward (5’ to 3’)	Reverse (5’to 3’)
Msk1	CAATGAATGGCTTCAGGATG	AAAGGCATGAAAGGTTGCTT
Gad1	AGCCTGAGCACACAAATG	TGACTCCATCATCAGAGCTT
Gad2	GTCTGCTTCTGGTTTGTACCT	GTGGTCCCATACTCCATCATTC
Gabrg3	GGAGCTGATGAACTTCAAATCG	GCAACCAGGAGGACAGAG
Drd1	ATGATCGTCACTTACACCAGTATC	TTCGACAGGGTTTCCATTACC
Drd2	ACATCTTTGTCACTCTGGATGTC	CCCAGACAATGGCGATCAT
Drd3	TTATCCACATCCCTGAAGCTG	ACAGTGGGTATTAAGAACGTGAG
Grin1	TGGAGAAGCACAATTATGAGAGT	CCAGATCGCACTTCTGTGAA
Psd95	ACTGCATCCTTGATGTCTCAG	TCCTCTGTGATCCGCTTATTG
5-Htrc2	GTCCCTAGCCATTGCTGATATG	AGCACATCTAGTGAAATCCAGAC
Irak1	GTCTTGGATAGCCTGCAACTG	TGAGGGATTTGTCAGAGTGAAC
Satb1	TCTAGGAAGAGGAAGGCTTGG	CGCAGAAAACTGGTAACATGG
Dlk1	TGTCAATGGAGTCTGCAAGG	ATTCGTACTGGCCTTTCTCC
Pvalb	GGACATCAAGAAGGCGATAGG	GGAACACCTTCTTCACCTCAT
Darpp-32	GGTCTCAGAGCACTCCTCACCAG	TGCTGCACAGCTTTCAGTGAT
Gfap	CACCTACAGGAAATTGCTGGAGG	CCACGATGTTCCTCTTGAGGTG
Ppargc1a	GAAATTGAGGAATGCACCGTAAA	CGACCTGCGTAAAGTATATCCA
Tbp	CACCAATGACTCCTATGACCC	CAAGTTTACAGCCAAGATTCACG

Supplementary Table 2: crRNAs used to generate the deletion of EXON IV.

MSK1-crRNA1	5'-GGGAGGGTTTGGTCGTCATGTGG-3'
MSK1-crRNA2	5'-AATCCCAGTACTTCATTAGGGGG-3'

Supplementary Table 3: Primers for genotyping *Msk1^{IV}* KO mice.

MSK1 Forward	CAGCCATTGTTGCATGGAAC
MSK1 Reverse	TACTGTACAGCATGGGCTTC

102 Forward	CGTCATGTGGCTGATGTTTG
103 Reverse	CATGGAGCAAGTCACAATCAAG
114 Forward	ATGGTTAGCCCAGAGTGATTAAA
115 Reverse	CATTCATAAGCCCAAGGCAAC

Supplementary Table 4: oligonucleotides used to generate the miRNA-based shRNAs.

shMSK1-1 top	TGCTGAGAATATGCTCTTTCAGTTTCGTTTTGGCCACTG ACTGACGAAACTGAGAGCATATTCT
shMSK1-1 bottom	CCTGAGAATATGCTCTCAGTTTCGTCAGTCAGTGGCCA AAACGAAACTGAAAGAGCATATTCTC
shMSK1-2 top	TGCTGTGAAGAGGATCTATAACAGCTGTTTTGGCCACT GACTGACAGCTGTTAGATCCTCTTCA
shMSK1-2 bottom	CCTGTGAAGAGGATCTAACAGCTGTCAGTCAGTGGCC AAAACAGCTGTTATAGATCCTCTTCAC
shMSK1-3 top	TGCTGAAAGGTTGCTTTCACACAGGTGTTTTGGCCACT GACTGACACCTGTGTAAGCAACCTTT
shMSK1-3 bottom	CCTGAAAGGTTGCTTACACAGGTGTCAGTCAGTGGCC AAAACACCTGTGTGAAAGCAACCTTTC
shMSK1- 4 top	TGCTGTACATTAGAACACCTAAGCTCGTTTTGGCCACTG ACTGACGAGCTTAGGTTCTAATGTA
shMSK1-4 bottom	CCTGTACATTAGAACCTAAGCTCGTCAGTCAGTGGCCA AAACGAGCTTAGGTGTTCTAATGTAC
shControl-LacZ top	TGCTGAAATCGCTGATTTGTGTAGTCGTTTTGGCCACTG ACTGACGACTACACATCAGCGATTT
shControl-LacZ bottom	CCTGAAATCGCTGATGTGTAGTCGTCAGTCAGTGGCCA AAACGACTACACAAATCAGCGATTTC

Supplementary Table 5: Primers for cloning of MSK1 and Sanger Sequencing and primers to generate the shRNA-resistant form mutMSK1 and mutMSK1myc.

MSK1-BamHI- Forward	cgggatccGAGGGTGAAGATGGAGGG
MSK1-NotI-Reverse	cggcggccgcTCAGTCTGAGAACTGGAAGAGGGTGTC
MSK1-NotI-*myc* Reverse	cggcggccgcTCA*cagatcctcttctgagatgagttttgttc*GTCTGAGAACTGGAAGAGGGTGTC
MSK1-440	GTTTCACAGAGCACGAAG
MSK1 -532	TAATGTCACGGTATATAATC
MSK1-995	AAGATAAAGTGGGATGAC
MSK1-1490	TGGAACTTCTGAATGGCG
MSK1-1964	TATCCCAAGAGGCTAAAG
mut-shM1	GGTCTGAGTAAGGAGTTTGTGGCCGATGAgACcGAgAGAGC
mut-shM2	GCGTAACGCAGCcGTCATcGAcCCTCTTCAGTTC
mut-shM3	GACTGGTGGAGCcTgGGTGTcCTAATGTATGAGCTAC
mut-shM4	GCTGTGCACACCTGcGTGAAgGCAACCTTTCATGCC
MSK1-NheI-Forward	gctagcGAGGGTGAAGATGGAGGG
MSK1-EcoRI-myc Reverse	cgaattctcAcagatcctcttctgagatgagtttttgttcGTCTGAGAACTGGAAGAGGGTGTC